DEVELOPMENT OF PARTICLE PLATFORMS FOR DELIVERY OF ANGIOGENIC REAGENTS TO TREAT PERIPHERAL ARTERIAL DISEASES

by

DUONG QUANG LE

DISSERTATION

Presented to the Faculty of the Graduate School of

The University of Texas at Arlington in Partial Fulfillment

of the Requirements

for the Degree of

DOCTOR OF PHILOSOPHY

THE UNIVERSITY OF TEXAS AT ARLINGTON

December 2018

Arlington, Texas

ACKNOWLEDGEMENTS

This work has been done with the financial support from Vietnamese-American bilateral funding, Vietnam Education Foundation, from the Department of Bioengineering, University of Texas at Arlington, and especially from my supervising professor, Dr. Kytai Truong Nguyen. All projects in this dissertation were supported partially by Dr. Nguyen's grant NIH R01 HL 118498.

I would like to sincerely appreciate professors Jun Liao, Liping Tang, and Baohong Yuan for being a committee member for my comprehensive exam and dissertation defense. I greatly appreciate their helpful advices and criticized concerns during my doctoral program to sharpen my research skills. I specially thank Dr Suchismita Acharya for a great collaboration, and I am delightful to join her in investigating new therapeutic agents SA-2 and SA-10 to treat PAD disease and more.

Under great collaboration with Ultrasound and Optical Imaging Laboratory (Department of Bioengineering, UTA), I would like to thank Wenbin Cai who taught me to make microbubbles, and I would like to give appreciation to Yang Liu for setting up ultrasound systems and performing ultrasound-related works for me. In addition, I also would like to acknowledge that microbubble-related works, including material synthesis and devices, were partially funded by CPRIT grant RP170564.

I am thankful to Amirhossein Hakamivala from Regenerative Medicine and Cancer Therapy Laboratory (Department of Bioengineering, UTA), who helped me with the tissue sectioning and staining. I thank to Yihui Huang for helping me with

supplies and equipment for animal studies. I especially appreciate Dr. Liping Tang who provided us access to Kodak *in vivo* imaging systems and uncountable times to help with issues relating animal studies. I also thank to Dr. Hao Xu who initially trained us with the surgery for PAD models.

I would like to appreciate my students, Phong (Daniel) Tran and Vy Tran who have worked very hard with me on the projects. I truly appreciate my labmates, Tam Nguyen, who helped me with animal surgeries among other studies, and Aneetta Kuriakose, who worked with me on SA-2 therapeutic evaluation and advised me with the binding antibodies. I am thankful to all of my other labmates in Nanomedicine and Tissue Engineering Lab who have helped me uncountably throughout my doctoral program.

Above all, it has always been my greatest appreciation to join Nanomedicine and Tissue Engineering Lab and to work under the supervision of professor Kytai T. Nguyen. I was given the biggest chance to discover many scientific aspects, to broaden collaborative network, and to strengthen critical thinking. I have been given the greatest support so far.

December 12, 2018

DEDICATION

I am whole-hearted thankful to my family, especially my mother, brother, sisters, wife, and son, who have always supported me to pursue my academic career.

With all love and remembering, I would like to dedicate this dissertation to my beloved father, the pioneer who took me to science, and who passed away because of cardiovascular disease that has been the great motivation for me to conduct this research.

Abstract

DEVELOPMENT OF PARTICLE PLATFORMS FOR DELIVERY OF ANGIOGENIC REAGENTS TO TREAT PERIPHERAL ARTERIAL DISEASES

Duong Le, MS

The University of Texas at Arlington, 2018

Supervising Professor: Kytai Truong Nguyen

Peripheral arterial disease (PAD) is a disease that one or several peripheral arteries are narrowed or blocked. PAD is an emerging disease that cost annually 10-20 billions of US dollars for health care in America. PAD patients suffer high risk of limb loss, amputations and mortalities. At 5 years, the amputation rate for PAD is 40%-70% while the 5-year survival rate is less than 30%. For PAD patients undergoing acute and critical limb ischemia, surgery bypass and endovascular balloon/stenting are applied as standard treatments. However, surgical bypass is subject to patients' readiness of autologous veins and the depth of arteries while endovascular intervention has limits due to complexes of specific arteries. More importantly, about 20-30% of PAD patients with critical limb ischemia cannot undergo surgery or endovascular revascularization. In this research, we have sought for an alternative treatment by utilizing nanoparticles that carry hybrid NO donor/antioxidant SA-2 and SA-10 molecules. The NPs were treated to animals under plain form and conjugation form with microbubbles. Results showed that our hybrid SA-10 NPs were able to recover animals both physically and physiologically. The research outcomes suggested the potentials of utilizing SA-10 NPs as a new treatment for PAD.

TABLE OF CONTENTS

LIST OF ILLUSTRATIONS

LIST OF TABLES

CHAPTER 1. PERIPHERAL ARTERIAL DISEASE: CURRENT ISSUES, ALTERNATIVE TREATMENTS, HYPOTHESIS AND DESIGN

1.1. INTRODUCTION

1.1.1. PAD definition, symptoms and classification

Peripheral arterial disease (PAD) is a disease that one or several peripheral arteries, which are not directly connected to heart (so-called noncardiac, nonintracranial arteries), are narrowed or blocked. PAD is commonly happened on lower extremities of the body. The annual cost for PAD-relating health care in US is $10-$20 billion dollars.[1] Of which, the overall costs per individual suffering critical limb ischemia (CLI), a subcategory of PAD, increased by 63% from $12,560 in 2001 to $20,517 in 2011.[2]

PAD is age-dependent and the majority of patients are recorded at middle-age. According to American Heart Association (AHA) statistics, about 8.5 million Americans over 40 years old[3, 4] and at least 200 million people worldwide[5] suffer from PAD. This has been accounted for an overall prevalence 12% in the American adult population,[1] and of which ~20% of individuals are over 70 years of age.[1] Atherosclerosis, an event that arteries have the deposition of substances such as cholesterol, fatty substances, cellular waste products, calcium and fibrin, is the main cause of PAD,[1, 6] and less common causes include inflammatory disorders of the arterial wall (vasculitis) and noninflammatory arteriopathies such as

fibromuscular dysplasia. Hypertension, obesity, dyslipidaemia, smoking, diabetes, coronary artery disease, chronic heart failure and chronic kidney disease are other causes of PAD. It is also noted that PAD currently presents in almost 40% of cardiovascular disease (CVD)-related diabetic cases[7] (**Fig. 1.1**), bearing to the fact that the number of diabetic patients is predicted to double by 2030.[8]

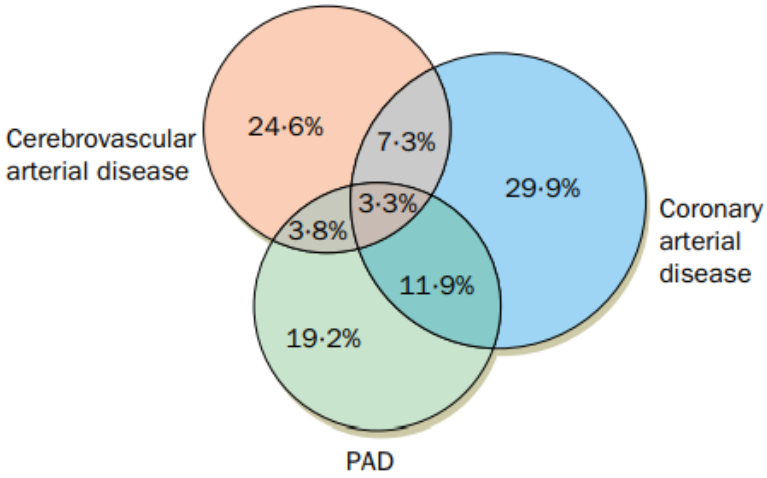

Figure 1.1. Occurrence of PAD represents in almost 40% of CVD-related diabetic diagnoses.[7]

It is recommended by AHA and American College of Cardiology (ACC) that the below populations carry high risks of PAD:[4]

- From 65 years old or older.
- Age 50–64 years old with family history of PAD or with risk factors for atherosclerosis (e.g., diabetes mellitus, history of smoking, hyperlipidemia, hypertension).
- Age <50 years old with diabetes mellitus and 1 additional risk factor for atherosclerosis.

- Individuals with known atherosclerotic disease in another vascular beds (e.g., coronary, carotid, subclavian, renal, mesenteric artery stenosis).

Patients suffered from PAD may express from no symptoms to symptoms of intermittent claudication (IC), leg pain, rest pain, ischemic ulcers, or gangrene.[1] Most commonly, symptoms of PAD are classified with Rutherford-Becker scale (**Table 1.1**) using Ankle-brachial index (ABI) plus toe pressure (TP).

Table 1.1. Classification of Peripheral Arterial Disease using Rutherford-Becker scale.[1]

Rutherford-Becker		**ABI or TP**	**Symptoms**
Grade	Category		
0	0	ABI > 0.95	Asymptomatic
I	1	ABI > 0.80	Mild claudication
I	2, 3	ABI > 0.40	Moderate-severe claudication
II	4	ABI < 0.40	Ischemic rest pain
III	5, 6	TP < 30 mm Hg	Tissue loss

Larger ABI means less severe symptoms while smaller ABI means more severe symptoms.

PAD is classified not only by symptoms but also, more importantly, by its severity. Clinically, the severity of PAD is classified into asymptomatic PAD, IC, acute limb ischemia (ALI) and CLI.[4] ALI is the stage that symptoms and hypoperfusion have been appeared for less than 2 weeks[4] while CLI is noted as the end stage of PAD, which has higher rate of limb loss and mortality. Further

classification has also been provided by AHA and ACC[4] including salvageable limb (curable motor functions under treatments), nonviable limb (loss of motor functions and neurological functions to partial or whole extremity, and tissue integrity cannot be restored with treatment) and tissue loss (from nonhealing ulcer and focal gangrene (minor severity) to non-salvageable to foot (major severity)).

Ischemia related to PAD occlusions has high rates of amputations and mortalities worldwide. Clinical research has reported that PAD patients having ABI<0.5 have higher rate (P<0.01) of limb loss (28% and 34% at 6 and 12 months, respectively) compared to ones having ABI>0.5 (10% and 15% at 6 and 12 months, respectively).[9] Overall amputation rates in PAD patients with CLI are 10%-40% at 1 year, 40%-70% at 5 years, and 80%-95% at 10 years. As a consequence, the leg amputation gives rise to a high mortality rate. The 1-year mortality rate of PAD patients with CLI is 20-25%, and annual mortality rates is 4-6%,[1] in which 13,854 American deaths in 2010 were recorded[3] according to AHA. The 5-year survival rate for PAD patients with CLI is less than 30%.[1]

1.1.2. PAD diagnosis

Currently, PAD could be detected with various non-invasive method such as ABI measurement, plethysmography and transcutaneous oximetry.[10] Among these, the ABI has emerged as an effective and precise method that not only qualitatively diagnoses the occurrence but also quantitatively gives the severity of PAD.[7, 10] The ABI is calculated as ratio of ankle systolic pressure measured with a

blood pressure at the malleolar level to the higher pressure of the two brachial arteries (**Equation 1.1**).

$$ABI = \frac{P_{\text{ankle systolic pressure}}}{P^{\max}_{\text{brachial artery}}} \qquad \text{(Equation 1.1)}$$

Simply, patients with ABI≤0.90 is considered to suffer PAD, specifically lower index indicates higher severity. Claudication occurs where ABI ranging from 0.5 to 0.9 while acute ischemia results in ABI<0.2 (**Fig. 1.2**).

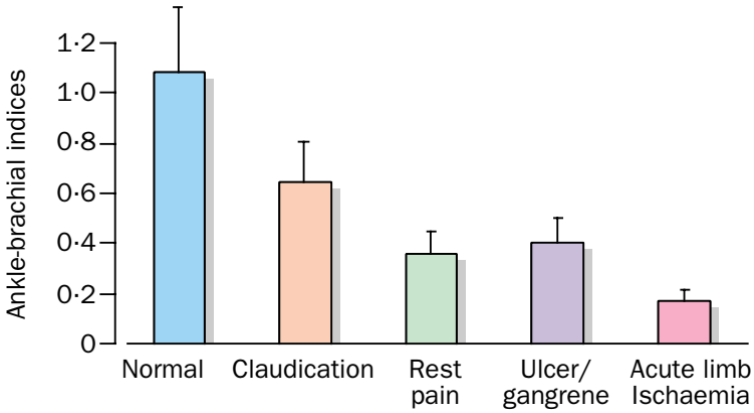

Figure 1.2. Using Ankle-brachial index (ABI) as an effective diagnosis tool for PAD. Lower ABI value indicates more severe PAD status.[7]

Besides ABI index, toe-brachial indexes (TBI) could be used in patients with poorly compressible arteries,[6] especially recommended when ABI>1.4.[4] Meanwhile, Doppler ultrasonography, color duplex scanning, magnetic resonance angiography and computational tomography angiography (CTA) provide structural images of patients' arteries (**Table 1.2**) and are able to detect atherosclerotic plaque in peripheral arteries.[6] These techniques, especially ultrasonography combined with Doppler imaging are commonly used to assess stent or graft patency after revascularization.[6]

Table 1.2. Recommended angiographic imaging[4] for suspected PAD patients.

Duplex ultrasound, CTA, or MRA of the lower extremities is useful to diagnose anatomic location and severity of stenosis for patients with symptomatic PAD in whom revascularization is considered
Invasive angiography is useful for patients with CLI in whom revascularization is considered.
Invasive angiography is reasonable for patients with lifestyle-limiting claudication with an inadequate response to GDMT for whom revascularization is considered.
Invasive and noninvasive angiography (i.e., CTA, MRA) should not be performed for the anatomic assessment of patients with asymptomatic PAD

CTA: computed tomography angiography; MRA: magnetic resonance angiograph; GDMT: guideline-directed management and therapy

In addition to indexing and imaging, exercise testing on a treadmill is recommended[4] when 0.9<ABI≤1.4 to measure severity of PAD from maximum walking times. **Table 1.3** lists the recommendations of AHA and ACC for physiological tests on suspected PAD patients.[4] Overall, combined diagnosis (**Fig. 1.3**) suggests appropriate treatments to the patients.

Table 1.3. Recommended physiological tests[4] for suspected PAD patients

Toe-brachial index (TBI) should be measured to diagnose patients with suspected PAD when the ABI is greater than 1.40
Patients with exertional non–joint-related leg symptoms and normal or borderline resting ABI (>0.90 and ⩽1.40) should undergo exercise treadmill ABI testing to evaluate for PAD
In patients with PAD and an abnormal resting ABI (⩽0.90), exercise treadmill ABI testing can be useful to objectively assess functional status
In patients with normal (1.00–1.40) or borderline (0.91–0.99) ABI in the setting of nonhealing wounds or gangrene, it is reasonable to diagnose CLI by using TBI with waveforms, $TcPO_2$, or SPP
In patients with PAD with an abnormal ABI (⩽0.90) or with noncompressible arteries (ABI >1.40 and TBI ⩽0.70) in the setting of nonhealing wounds or gangrene, TBI with waveforms, $TcPO_2$, or SPP can be useful to evaluate local perfusion

$TcPO_2$: transcutaneous oxygen pressure; SPP: skin perfusion pressure

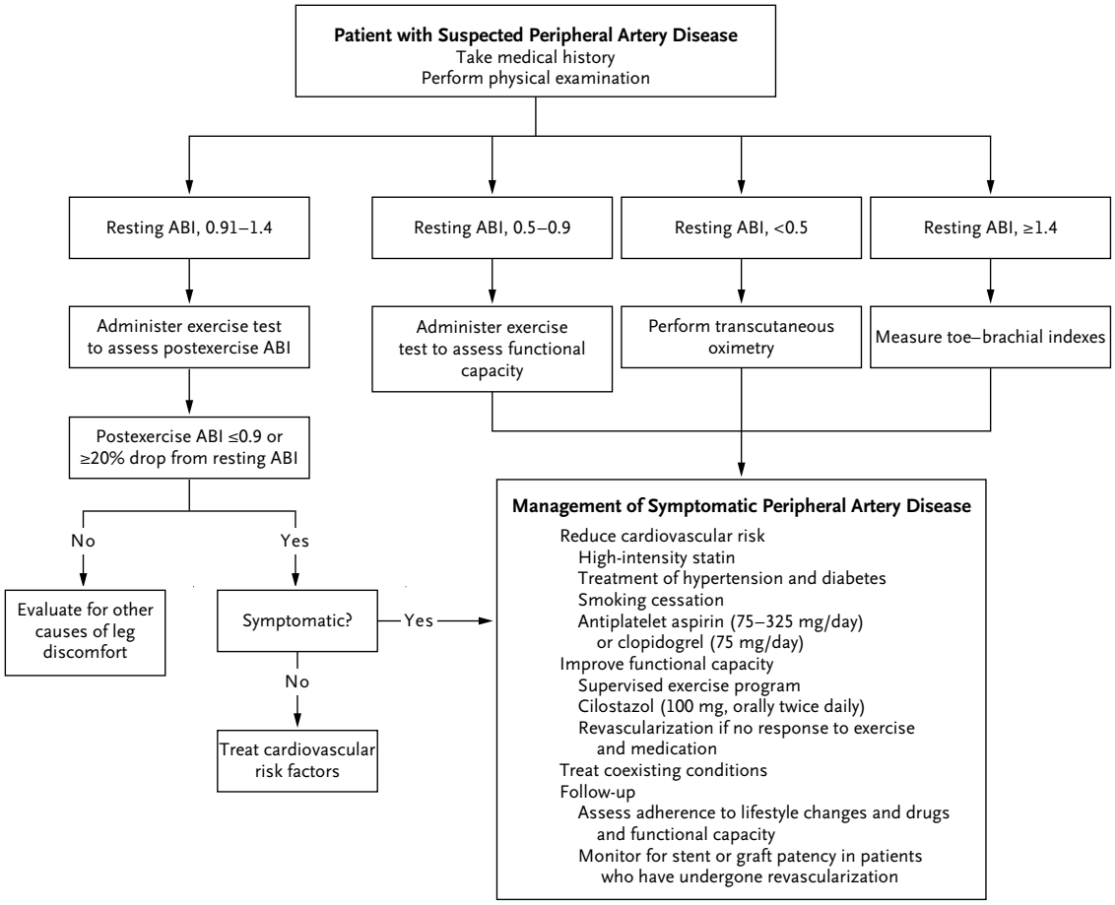

Figure 1.3. Suggested approach to the evaluation and treatment of patients with PAD.[6] Reproduced with permission from scientific reference citation, Copyright Massachusetts Medical Society.

1.1.3. Current treatments and limitations

Variative traditional approaches such as lifestyle changing, bypass grafting, and endovascular interventions have been used to treat PAD (**Fig. 1.4**). The lifestyle changing starts with a routine exercise that subsequently helps bring lipids, blood pressure, and blood sugar under control.[7] Since smoking stands as an important cause to PAD, it is crucial that patients should cease completely from tobacco use.[4, 7] Pharmacotherapy, including but not limited to antiplatelet and

statin agents, antihypertensive agents, cilostazol and influenza vaccination,[4] could be used under medical supervision.

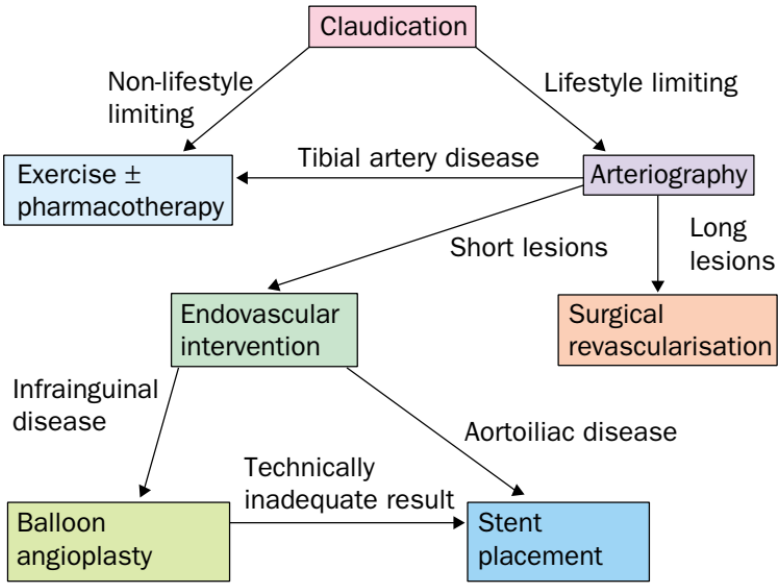

Figure 1.4. Traditional treatment procedures for PAD patients suffering claudication.[7]

Antiplatelet (e.g. aspirin and clopidogrel) reduces risks of myocardial infarction (MI), stroke, and vascular death to both symptomatic and asymptomatic PAD[4] while treatment with a statin medication is indicated for all patients with PAD.[4] Antihypertensive agents also reduce the risks of MI, stroke, heart failure, and cardiovascular death.[4] Meanwhile, cilostazol helps improve symptoms and increase walking ability to PAD patients with claudication.

For PAD patients with lifestyle-limiting claudication and inadequate response to GDMT,[4] revascularization is recommended. For PAD patients that have undergone claudication and CLI, revascularization, including endovascular treatment and surgical bypass, is considered as standard treatments.[1] Endovascular revascularization for claudication includes balloon dilation

(angioplasty), cutting balloons, drug-coated balloons, covered stents, drug-eluting stents, and atherectomy, and the choice of revascularization means depends on the type and position of lesions. In general, endovascular procedures are effective for claudication due to hemodynamically significant aortoiliac occlusion, hemodynamically significant femoropopliteal occlusion or unknown occlusion on isolated infrapopliteal artery.[4] The therapeutic efficacy of endovascular intervention, however, is limited due to late restenosis. Another effective approach is surgical intervention or so-called surgical bypass. The surgical bypass is usually performed on femoral and proximal popliteal arteries where stenosis and occlusion commonly happen among individuals with claudication.[4] The type of conduit is recommended with autogenous vein in preference to prosthetic graft materials.[4] Although patency outcomes for surgical interventions might be better than endovascular treatments in term of patency for claudication events,[4] surgical interventions still associate with greater risk of adverse perioperative events. Thus, it is only performed to individuals who do not respond to nonsurgical therapies and possess favorable arterial anatomy to surgery. It is not recommended by AHA and ACC to perform femoral-tibial artery bypasses with prosthetic graft materials for the treatment of claudication.[4]

Similar to claudication, CLI requires either surgical or endovascular revascularization to provide in-line blood flow to the foot. Initially, autologous vein bypass transplantation is considered as the first line therapy in PAD.[7] Recently, however, the Bypass versus Angioplasty in Severe Ischemia of the Leg (BASIL)

suggested that endovascular revascularization is more effective than open surgery for patients with CLI.[4, 11] It has been reported that a 3-fold increase in endovascular revascularization[12] for PAD patients with CLI from 1996-2006, and it was doubled (from 13.4% to 27.4%)[2] for the period 2001-2011. Clinically, the endovascular revascularization is recommended for patients with ischemic rest pain, nonhealing wounds, or gangrene. **Figure 1.5** presents lesion sites and appropriate materials for endovascular revascularization for patients with CLI.[6]

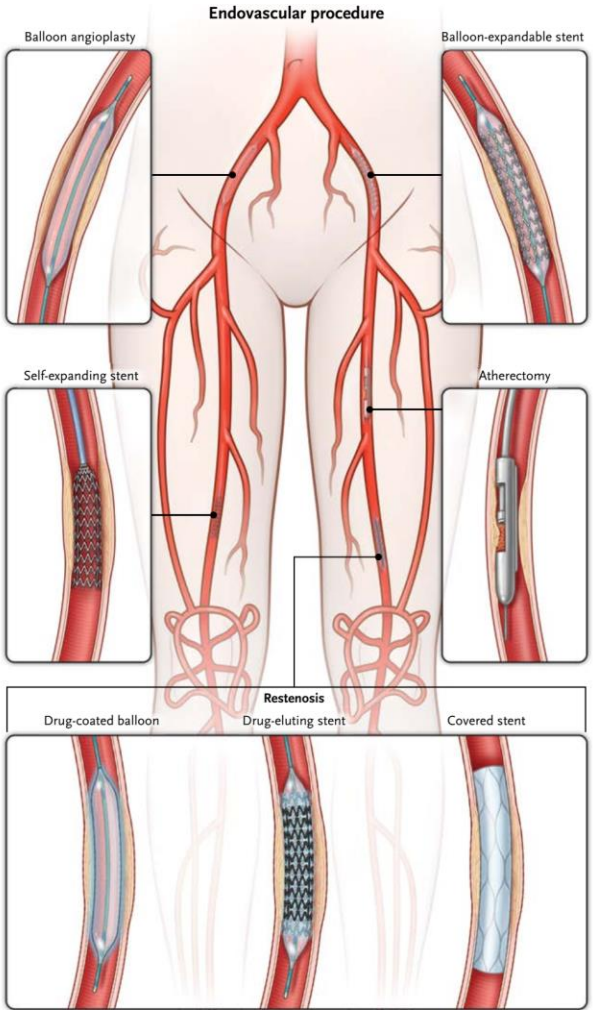

Figure 1.5. Major arteries of the legs and endovascular revascularization for the treatment of PAD.[6] Reproduced with permission from scientific reference citation, Copyright Massachusetts Medical Society.

Meanwhile, surgical bypass is recommended when endovascular revascularization has failed for patients with CLI.[4, 6] The bypass to the popliteal or infrapopliteal arteries is recommended with suitable autogenous veins.[4] The saphenous vein is the preferred conduit for infrainguinal bypass,[6] while a prosthetic conduit can be used for femoral-popliteal bypass. Femoral-tibial artery bypasses with prosthetic graft materials are accepted under AHA/ACC guidelines once autologous veins are not available.

The revascularization, either by endovascular or surgical techniques, helps patients to restore with sufficient blood perfusion to lower extremities upon success. Nevertheless, the intervention often causes thrombosis and restenosis.[13] In fact, revascularization as a sole treatment for PAD patients has been questioning, and a combination of treatments has been considered. Kenneth Ouriel[7] mentioned about the introduction of antithrombotic reagents (such as Heparin) or antiplatelet (such as Aspirin) during and after surgery to improve treatment efficacy and avoid side effects. More importantly, there is a high number of 20%-30% of PAD patients with CLI who are not suitable candidates for surgery or endovascular revascularization. These facts indicate the importance in the development of an alternative therapy to treat PAD where patients do not have to undergo any surgery.

1.1.4. Other approaches to treat PAD

Recently, new approaches to treat PAD that avoid intervention and/or operation have raised more attention from scientists. The non-surgical treatment include i) introduction of living stem cells (SCs) to cure lesions, and ii) investigation of small drugs (e.g. antiplatelet reagents,[10] fibrinogen inhibitors,[10] nitric oxide donors and antioxidants) and growth factors (e.g. vascular endothelial growth factor (VEGF), basic fibroblast growth factor (bFGF), hepatocyte growth factor (HGF) and nerve growth factor (NGF)) that participate in the formation new blood vessels.[10]

Living SCs have attracted attention due to their potential of homeostasis, pro-angiogenesis and differentiation into other cell types, including endothelial cells (ECs). For instance, endothelial progenitor cells (EPCs) play important roles in cardiovascular regeneration in several mechanisms. Under direct contacts with EPCs, injured ECs at lesions upregulated adhesion molecule expression and nitric oxide synthase (NOS) activities,[14] thus injured ECs were either repaired or replaced with new ECs. Under indirect contacts, ECs received paracrine proangiogenic signals that induce the formation or new vessels. Moreover, a subtype endothelial colony-forming cells (ECFCs), so-called late EPCs, possesses an intrinsic property of neoangiogenesis,[15, 16] especially under ischemia injuries.[17] Specifically, ECFCs not only differentiate into mature ECs but also incorporate into newly formed vessels[18] for the treatment of diabetes mellitus and PAD. Similarly, it has been reported that adipose-derived SCs not only sent paracrine signals toward injured ECs to repair and induce angiogenesis[19, 20] but also differentiated

into cardiomyocytes and vascular cells to cure cardiovascular-related diseases.[21] Although SCs carry enormous potentials, some major concerns have been raised. Living SCs have poor retention time[22] where they are easily attacked and cleared out by the immune system. More importantly, it has been proved that some cancers have been originated from either undifferentiated or overactivated self-renewal SCs.[23]

Besides living SCs approach, angiogenic particulates have also been investigated. It has been reported that, either supplying NO or scavenging ROS played important roles in inducing angiogenesis.[24] While these therapeutic reagents, including growth factors, could be administered in free form, they are either unstable or quickly cleared out *in vivo*. Nanoparticle research has helped in increasing therapeutic efficacy. Basically, nanoparticles (NPs) are defined as polymeric particulates at sub-micron size[25] or typically less than 500 nm.[26] However, it is generally accepted that NPs are particles that have at least one dimension less than 100 nm,[27] and combined effective dimensions less than 200 nm for medicinal applications.[26] Due to small sizes, NPs have a relatively large surface, which allows NPs to either conjugate, adsorb therapeutic agent(s) or surface modified with targeting ligands. The therapeutic agents could also be loaded within polymeric matrix of NPs. Generally, therapeutic efficacy is increased by several mechanisms as follow: NPs protect drugs from enzymatic and chemical degradation and increase their half-life;[28] decrease immunological and renal clearance;[28, 29] increase accumulation of drugs in diseased tissues;[28] provide

sustained release[28, 29] or responsive-release to pH, temperature, enzymes, external magnetic fields, light, and radiofrequency;[30, 31] tailor biocompatibility and reduce cytotoxicity to healthy tissues.[32] However, the main hindrance for the treatment via NPs is the deliver-on-demand where NPs are needed to specifically localize at the injury and activate the effects; rapid clearance might happen before the therapeutics take effects.[33] While the targeting issues could be somehow solved by introduction of antibodies that selectively bind to ischemia- and diabetes-inducing receptors such as hypoxia-inducible factor (HIF)-1,[34] intercellular adhesion molecule (ICAM)-1,[35, 36] vascular cell adhesion molecule (VCAM)-1,[35, 36] newly reported circulating fatty acid synthase (cFAS),[37] and fatty acid-binding protein 4 (FABP4),[38] an on-demand-release has not been met in PAD treatment. On another mainstream, cancer treatment has utilized image guide delivery system to increase controlled release of drugs upon delivery. Namely, magnetic nanoparticles binding air microbubbles,[39, 40] doxorubicin loaded microbubbles,[41] and nucleic acid loaded microbubbles[42, 43] and other form of ultrasound (US) assisted delivery[44] have been reported for cancer treatment. Although tissue regeneration and anticancer have different interests in cell and tissue behaviors, the concept of image-guide delivery remains, and it is believed that US could provide the controlled over delivery of nanoparticles to the ischemic region and locally trigger the release on demand.

1.2. HYPOTHESIS

- Simultaneously supply NO and scavenge ROS could protect ECs from ischemic events and induce angiogenesis.
- Loading a novel hybrid molecule with dual functional NO donor/antioxidant in NPs and delivering them at the ischemic site help protect drugs and prolong their therapeutic effects.
- Incorporating NPs with MB could enhance therapeutic efficiency in PAD treatment

1.3. OBJECTIVES

Our objective was to treat PAD by fabricating angiogenic nanoparticles that are consisting of NO donor/antioxidant, were surface-modified through receptor/ligand bindings. In addition, an ultrasound transducer also introduced ultrasound stimulation at the ischemic region for triggering the release of these NPs to enhance the therapeutic efficacy.

1.4. SPECIFIC AIMS

To fulfill our objectives, three specific aims had been proposed

Aim 1: To synthesize the first generation of NPs that possess both NO donor and ROS scavenging abilities. *In vitro* characterization studies have been performed to test the therapeutic effects on vascular cell functions.

Aim 2: To conjugate angiogenic NPs on microbubbles. Characterization and *in vivo* studies have been performed on PAD mouse models to evaluate for their therapeutic efficacy.

Aim 3: To synthesize the second generation of NPs that possess both NO donor and ROS scavenging abilities. *In vitro* and *in vivo* characterization studies have been performed to determine the effectiveness of these NPs in the treatment of PAD.

We focused on utilizing nanoparticles to investigate therapeutic effects *in vitro* and *in vivo* without any other stimulation, and with US stimulation. The purpose of testing without stimulation was to understand how cells and animals are being cured by regulating NO and ROS levels under ischemic conditions, since NO and ROS plan important roles in endothelial cell functions and ischemic events, respectively. Next, once we have confirmed that the NO and ROS levels simultaneously played key roles in functions of endothelial cells and recovery of ischemia in animals, we sought for an improved treatment where the MB-NPs in general and NPs in specific were further investigated (**Fig. 1.6**).

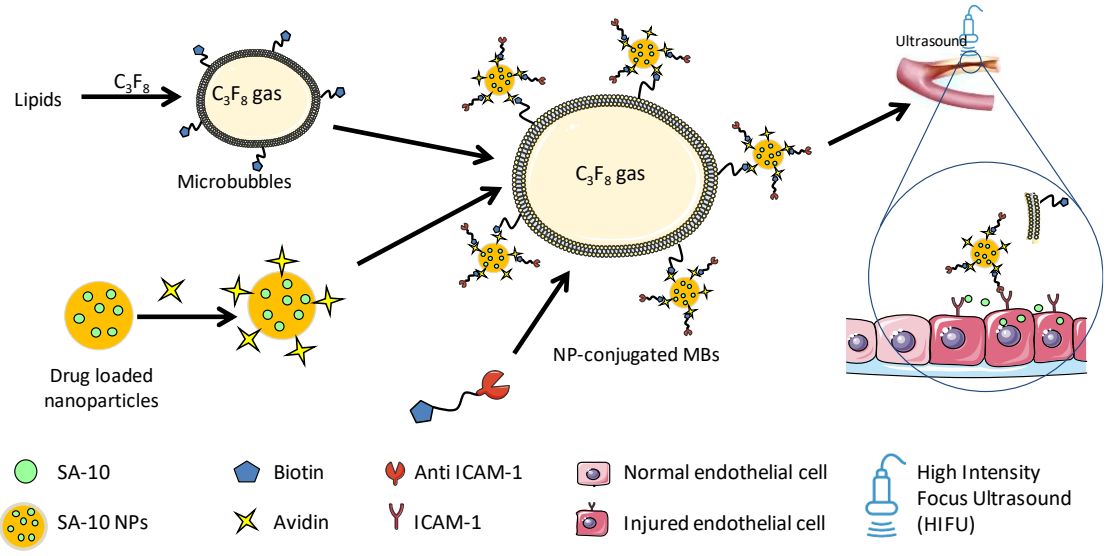

Figure 1.6. Schematic of MB-NP delivery system via stimulation of focused ultrasound. DPPC and DSPE-Biotin were mixed in chloroform, evaporated to form thin films, hydrated in buffer and introduced C_3F_8 gas prior to amalgamation to make microbubbles. The microbubbles were conjugated with avidin-tagged NPs to form NP-conjugating microbubbles. Finally, MB-NPs were introduced to high pressure ultrasound (HIFU) to induce the release of drug-loaded NPs.

1.5. INNOVATION AND IMPACTS

Single application of either NO donor or antioxidant has been studied for PAD treatment by scientists. Yet it still remains drawback that oversupply of NO leads to elevation of ROS, which reverses the therapeutic effects, whereas only ROS scavenger does not facilitate EC functions, including angiogenesis. Our investigation is focused on improving endothelial dysfunction and blood flow in ischemic tissues. Here, we have investigated novel and innovative hybrid small molecules *in vitro* with the capability to inhibit the oxidative stress-induced endothelial dysfunction by scavenging the ROS and to facilitate new blood vessel formation.

Results from our work highlighted the important roles of both NO donors and antioxidants in protecting ECs and facilitating angiogenesis under stress conditions, including those in ischemic sites. Our work also highlighted the importance of utilizing nano-microparticles to provide sustained release of the drug over days and an emphasis of intramuscular administration to the site of injury. By this, we observed the recovery of animals in term of vasculogenesis, physiological blood perfusion indexes and physical ability to walk. Our work has initiated a new strategy of applying nanoparticles and image-guided nanoparticles for the treatment of PAD. If success, our research would provide an alternative therapy to effectively treat PAD in the future. Subsequently, the new method would benefit a vast majority of PAD patients, who are getting old and unable to adapt surgery and endovascular intervention. Consequently, lower death and mobility rates in addition to a higher life expectancy for PAD patients would be achieved.

CHAPTER 2. FIRST GENERATION SA-2 NANOPARTICLES FUNCTION AS BOTH NO DONORS AND ROS SCAVENGERS

COPYRIGHT AND PERMISSION

This chapter used contents in partial and full of our published research article below

Hybrid Nitric Oxide Donor and its Carrier for the Treatment of Peripheral Arterial Diseases

Duong Le,[‡] Aneetta Kuriakose,[‡] Dat Nguyen, Kytai Nguyen[*] & Suchismita Acharya[*]

Scientific Reports. Volume 7, Article number: 8692 (2017)

[‡]Co-first authors

[*]Co-corresponding authors

Under the permission of co-authors and open access permission of the publisher

Author information

Duong Q. Le and Aneetta E. Kuriakose contributed equally to this work.

Affiliations

Department of Bioengineering, University of Texas at Arlington, Arlington, TX, 76010, USA
Duong Q. Le, Aneetta E. Kuriakose, Dat X. Nguyen & Kytai T. Nguyen

Joint Biomedical Engineering Program, University of Texas Southwestern Medical Center, Dallas, TX, 75390, USA
Duong Q. Le, Aneetta E. Kuriakose, Dat X. Nguyen & Kytai T. Nguyen

North Texas Eye Research Institute, University of North Texas Health Science Center, Fort Worth, TX, 76107, USA
Suchismita Acharya

Contributions

D.L. and A.K. contributed equally to all the studies. D.N. contributed to the nanoparticle synthesis and characterization studies. All authors contributed to the manuscript and revision. S.A. and K.T.N. were responsible for final editing.

Competing Interests

The authors declare that they have no competing interests.

Corresponding authors

Correspondence to Kytai T. Nguyen or Suchismita Acharya.

Electronic supplementary material

Supplementary Figures

Rights and permissions

This page is available in the following languages:

Creative Commons License Deed

Attribution 4.0 International (CC BY 4.0)

This is a human-readable summary of (and not a substitute for) the license.

You are free to:

Share — copy and redistribute the material in any medium or format

Adapt — remix, transform, and build upon the material

for any purpose, even commercially.

The licensor cannot revoke these freedoms as long as you follow the license terms.

Under the following terms:

Attribution — You must give appropriate credit, provide a link to the license, and indicate if changes were made. You may do so in any reasonable manner, but not in any way that suggests the licensor endorses you or your use.

No additional restrictions — You may not apply legal terms or technological measures that legally restrict others from doing anything the license permits.

Notices:

You do not have to comply with the license for elements of the material in the public domain or where your use is permitted by an applicable exception or limitation.

No warranties are given. The license may not give you all of the permissions necessary for your intended use. For example, other rights such as publicity, privacy, or moral rights may limit how you use the material.

2.1. INTRODUCTION

It has been mentioned earlier that PAD is an emerging disease, having 8-10 million patients in the US and 200 million patients worldwide. Within the US, the annual health care for PAD reaches 10-20 billion US dollars with individual burdens peak at more than 20 thousand US dollars. Ischemia related to PAD occlusions carries high rates of limb loss, amputations (40%-70% at 5 years) and mortalities (20-25% at 1 year and 70% at 5 years for PAD patients suffering CLI) worldwide. Common treatments such as bypass grafts, endovascular and percutaneous interventions are feasible methods in restoring sufficient perfusion to maintain normal vessel functions, yet they often cause frequent late thrombosis and restenosis in arteries.[13, 45] Surgical bypass is subject to patients' readiness of autologous veins while endovascular intervention has limits due to complexes of specific diseases (specific arteries). Overall, there are as high as 20-30% of PAD patients with CLI are not suitable candidates to undergo either surgery or endovascular revascularization. These facts indicate the importance in the development of an alternative therapy to treat PAD.

Recently, therapeutic angiogenesis, the sprouting of new blood vessels from pre-existing vasculatures,[46] has proven to be a potential strategy to mitigate PAD patients' symptoms as it promotes vessel formation and lowers blood pressure while supplying oxygen-rich blood and nutrients to tissues in deficits.[47] This treatment route requires the administration of exogenous pro-angiogenic factors to trigger EC proliferation and migration and to remodel the extracellular

matrix (ECM) for tubule formation and expansion.[48] Another strategy is targeting the nitric oxide-cyclicguanosine monophosphate (NO-cGMP) pathway.[49-51] NO acts as an important signaling molecule regulating vascular inflammation,[52, 53] platelet function,[53] angiogenesis,[54] and protection from ischemia reperfusion injury;[55, 56] however, it is impaired in PAD.[57] Currently, many research studies have shown that although the supply of NO is important to ECs, it is crucial to maintain NO concentration at the physiological level. Excessive NO supply expands the NO gradient between extracellular and endogenous levels that consequently leads to ROS elevation, EC dysfunction[58] and poor endothelial progenitor cells' (EPCs) viability.[59] These observations suggest that using an NO donor that can provide a physiological concentration of NO might be effective for the treatment and prevention of PAD.

Besides regulating NO levels, reactive oxygen species (ROS) also play an important role in PAD pathology.[60] The ROS, including superoxide ($O_2^{\cdot -}$), peroxynitrite ($ONOO^{\cdot -}$), hydroxyl group ($OH^{\cdot}$) and hydrogen peroxide (H_2O_2), are regulated by body antioxidants such as superoxide dismutase, glutathione, glutathione peroxidase, catalase and so on.[61] In peripheral ischemia, a shortage of oxygen puts cells under oxidative stress, which in turn elevates ROS levels at the injured site. In addition, EC dysfunction at the injured site causes inflammation that recruits immune cells and produces more ROS. Additional superoxide also diminishes the NO bioavailability by forming toxic $ONOO^{\cdot -}$. When the ROS level exceeds the antioxidants produced in the body, more EC dysfunction and smooth

muscle cell (SMC) recruitment might occur.[62] Consequently, the accumulation of EC dysfunction and SMC migration leads to atherosclerosis and/or chronic inflammatory conditions.[63] Thus, the addition of antioxidants to NO donor is expected to reduce damage in ECs from oxidative stress.[64, 65]

In the present study, we synthesized a new compound, denoted as SA-2 (**Fig. 2.1**), that combined "spontaneous" NO donor[66] and superoxide dismutase (SOD) mimetic (nitroxide) functional groups and investigated their NPs in maintaining therapeutic levels of NO and scavenging superoxide.[67] The synthesized compound[68] SA-2 was investigated on inhibiting SMC migration and proliferation as well as preventing EC dysfunction compared to a standard pH-responsive NO donor (SIN-1)[68], nitroxide antioxidant (SA-3)[68] and mitochondrial enzymes-dependent hybrid compound (SA-5)[69]. A sustainable delivery system consisting of SA-2, SA-2-loaded PLGA nanoparticles (SA-2 NPs), was also synthesized, characterized and confirmed for a sustained release of SA-2 to further provide the improved EC survival and enhanced angiogenesis under stress conditions.

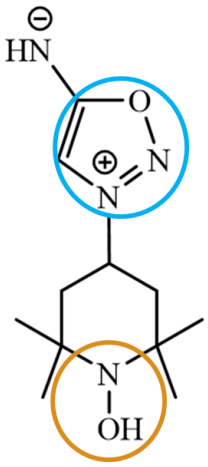

Figure 2.1. Structure of SA-2 that contains NO donor (Blue circle) and ROS scavenger (orange circle) functional groups

2.2. MATERIALS AND METHODS

2.2.1. Chemicals and reagents

Compound SA-2 was prepared in our laboratory as described previously.[67] Compound SIN-1 and SA-5 were prepared following literature procedures with >95% purity[70,71]. Compound SA-3 was purchased from TCI (Portland, OR). GW0742 was obtained from Tocris Bioscience (Bristol, UK). Chloroform and hydrogen peroxide (3%) were bought from Sigma-Aldrich (St. Louis, MO), and were ready to use without further purification. PLGA with copolymer ratio 50:50 and inherent viscosity of 0.4 dL/g was received from Lakeshore Biomaterials (Birmingham, AL). Carboxy-H_2DCFDA was purchased from Molecular Probes (Paisley, UK). MTS (CellTiter 96®Aqueous One Solution Cell Proliferation Assay) assay kits were purchased from Promega (Madison, WI). Cultrex Basement Membrane Extract was obtained from Trevigen (Gaithersburg, MD). OxiSelect™ Intracellular Nitric Oxide (NO) Fluorometric Assay Kit was ordered from Cell Biolabs (San Diego, CA).

2.2.2. Fabrication of SA-2 NPs

SA-2 loaded PLGA NPs were prepared using the standard single emulsion technique developed in our laboratory.[72-80] In brief, 10 mg of SA-2 was dissolved in 3 ml of chloroform containing 100 mg of PLGA to form an oil phase. This solution was then added dropwise into 20 ml of 5% PVA solution (water phase) and emulsified at 30W for 5 minutes to form the SA-2 loaded nanoparticles. The final emulsion was stirred overnight to allow solvent evaporation. The nanoparticles were washed and collected by ultracentrifugation and lyophilization before use.

2.2.3. Characterization of SA-2 NPs

Size of SA-2 NPs were characterized by dynamic light scattering (Brookhaven Instruments, ZetaPALS) and TEM images (Hitachi, H-9500). The stability of SA-2 NPs in media with serum were quantified by ZetaPALS in terms of the size change after incubating of these NPs in the solvent over predetermined time points.

The drug loading efficiency and drug release of SA-2 NPs were quantified by absorbance measurement of SA-2 contents. In brief, SA-2 standard solutions were subjected to wavelength absorbance scanning. After scanning, the wavelength of 230 nm gave the peak reading and absorbance at 230 nm of SA-2 at different concentrations were used for plotting a SA-2 standard curve with a linear regression equation. Using this equation, amount of unloaded SA-2 in supernatant was measured and the loading efficiency was calculated as 56% using the following equation:

$$\text{Loading efficiency}(\%) = \frac{\text{Total amount of drug used-Unloaded amount of drug}}{\text{Total amount of drug used}} \times 100\% \qquad \text{(Equation 2.1)}$$

For the drug release study, SA-2 NPs were suspended in the phosphate buffer saline (PBS) solution at 1 mg/ml concentration, placed in a dialysis bag with MWCO 5000 Da, and incubated at 37^{o}C over a time range. At each time point, a fixed volume of dialysate solution was pooled and replaced with the same volume of fresh PBS. Each sampling solution was then read for its absorbance value and the amount of released SA-2 was quantified based on standard curve mentioned

above. Consequently, a cumulative release profile of SA-2 was plotted. Study was repeat triplicate and data plot was mean values ± standard error.

The aqueous chemical stability of SA-2 ($t_{1/2}$) was determined using Liquid Chromatography-Mass Spectroscopy on Shimadzu LC/MS-2020, while circulation stability of NPs was quantified in terms of size change by DLS as mentioned earlier.

2.2.4. Doses and groups of study

For all studies unless otherwise mentioned, the no treatment (N/T) group was cells exposed to H_2O_2 only, while cells grown in complete media without exposure to anything served as a control group. Therapeutic drug, SA-2, was studied at concentrations of 0.05 µM, 0.5 µM and 5 µM. SIN-1, SA-3 and SA-5 were studied at a concentration of 50 µM according to effective concentrations mentioned in the discussion section. For therapeutic study of SA-2 NPs, the concentration of NPs used was based on the released SA-2 amount equivalent to the amount of free SA-2. To this, SA-2 NPs were used at SA-2 concentrations of 0.05 µM, 0.5 µM and 5 µM for all studies except the angiogenesis study (where 0.05 µM, 0.25 µM, 0.5 µM and 1 µM were used).

2.2.5. Media and cell lines

HUVECs and HASMCs were purchased from American Type Culture Collection (ATCC, Manassas, VA), while culture media (Vasculife Basal Medium) and supplemental kits (Vasculife VEGF Lifefactors for HUVEC, Vasculife SMC

Lifefactors for HASMC) were purchased from Lifeline Cell Technology (Frederick, MD). HUVECs and HASMCs cultured in complete media with 2% and 5% supplemented serum, respectively, were used as controls for our experimental studies. For experiments, all the treatment groups (SA-2, SIN-1, SA-3, SA-5 and SA-2 NPs) under stress conditions were cultured in low serum media (0.2% and 0.5% supplemented serum for HUVECs and HASMCs, respectively) at 37^0C.

2.2.6. Cellular stress conditions

Cell behavior was investigated under stress conditions with exposure to either H_2O_2 or hypoxia.

Oxidative stress: Pilot studies with different concentrations of H_2O_2 (0-400 µM) were added to ECs over various time ranges (4-24 hours), and the cell viability was assessed by MTS assays. Results showed that exposure to 400 µM H_2O_2 in 24 hours significantly reduced EC viability. Therefore, experiments associated with cell viability, the exposure of 400µM of H_2O_2 for 24 hours was chosen as an oxidative stress condition for ECs. In the angiogenesis and migration studies, the concentration of H_2O_2 was reduced to 200 µM to avoid biased results due to the cell death.

Hypoxic stress: Cells were subjected to 1% O_2 and 5% CO_2 at 37ºC to mimic chronic hypoxia in PAD per literature protocol,[81] whereas the cells exposed to 21% O_2 and 5% CO_2 served as a control (normoxic condition).

2.2.7. Assessment of eNOS levels in EC

Cells were seeded and allowed to attach on tissue culture well plates at a density of 20000 cells/cm^2. After incubation, cells were co-treated in 24 hours with H_2O_2 and either SA-2 at different concentrations, SIN-1 or SA-5. Cells treated with the NOS inhibitor L-NNA (N5-[imino(nitroamino)methyl]-L-ornithine) at 50 µM and no H_2O_2 served as NOS reference groups. After 24 hours of incubation, cells were washed several times with Dulbecco's Phosphate-Buffered Saline, and the eNOS level in cell sample was quantified with Intracellular Nitric Oxide Fluorometric Assay Kit following manufacturer's manual. In brief, the NO probe (provided with the kit) diffuses into cells and is deacetylated by cellular esterases to a non-fluorescent intermediate, then it is rapidly oxidized by intracellular nitric oxide to a triazolo-fluorescein analog and emits high fluorescence. The fluorescence intensity is proportional to the NO levels within the cell cytosol.

2.2.8. Determination of ROS Activity

Cells were co-treated with H_2O_2 and antioxidants (SA-2 at different concentrations, SA-3 or SA-5). After 24 hours of treatment, cytosolic ROS levels were measured using Carboxy-H_2DCFDA following the manufacturer's protocol on a UV–vis spectrometer (Infinite M200 plate reader, Tecan, Durham, NC) at a wavelength of 485/530 nm (Ex/Em). Fluorescence intensities of DCF proportionated to the cytosolic ROS.

2.2.9. Cell Viability Studies

Cells (HUVECs or HASMCs) were co-treated with H_2O_2 and either the hybrid drug SA-2 or reference compounds (SIN-1, SA-3, or SA-5). Due to fast hydrolysis of spontaneous NO donor such as SA-2 and SIN-1, all groups were refreshed with treatment reagents every 12 hours. After 24 hours of treatment, cell viability was quantified using MTS assays following the manufacturer's instructions.

2.2.10. Cell Migration Studies

To see the effects of SA-2 on the migration of HUVECs and HASMCs, *in vitro* scratching assays using these cells were performed. 20,000 cells/well were seeded onto 48-well tissue culture plates and incubated for 24 hours. Then using a 1000µl pipette tip, a 0.5 mm gap was made in each well, and images were captured using a phase contrast microscope. Cells were then co-treated with H_2O_2 and the therapeutic drugs as described earlier. All groups were refreshed with treatment reagents every 12 hours. After 24 hours of treatment, cells were stained with crystal violet and imaged again. The average distance or width of the gap before and after the treatment was determined using ImageJ software. The percentage of wound closure was quantified as below:[82, 83]

$$\text{Wound closure } (\%) = \frac{\text{Distance before migration-Distance after migration}}{\text{Distance before migration}} \times 100 \qquad \text{(Equation 2.2)}$$

2.2.11. Effects of SA-2 NPs on EC responses

HUVECs were exposed to SA-2 NPs, SA-2 drugs and co-treated with H_2O_2. After 1 and 4 days, cell viability was quantified using MTS assays and converted to a cell number based on the same linear fit curve of different cell numbers. EC viability was presented as number of cells that grew.

2.2.12. In vitro angiogenesis studies

Cultrex gel (liquid form) was coated onto 24-well plates and allowed to gel for 30 minutes at 37°C. HUVECs suspended in basal media (Vasculife) were seeded onto gel coated well plates at a seeding density of 25,000 cells/cm^2. For effects of SA-2, the cells were co-treated with SA-2 and 200 µM H_2O_2. Cells treated with either GW0742 (1 µM) or VEGF (25 ng/ml) served as positive controls, whereas cells exposed to H_2O_2 at 200 µM without any treatment served as negative controls (N/T). After 8 hours of treatment, the tube formation was imaged randomly (at least 10 areas for each group) using a phase contrast microscope. As the gel starts to disintegrate at 16 hours, an angiogenesis study over an extended period of treatment was not conducted.

For SA-2 NPs, since the SA-2 free drug exhibited the best results at 0.5 µM, NPs were studied at 0.25, 0.5 and 1 µM co-treated with 200 µM H_2O_2. A similar study was performed on NPs at 0.05 and 0.5 µM under hypoxic stress conditions. In this study, positive controls were cells treated with either GW0742 (1 µM) or VEGF (25 ng/ml) under hypoxic conditions while N/T was cells under hypoxic conditions without any treatment. The images taken were analyzed using

angiogenesis analysis tools in ImageJ software, and the length of the tubes (μm) was measured to determine the potential angiogenesis.

2.2.13. Statistical analysis

All the experiments were performed with n = 3÷6. Data were expressed as mean ± SEM. The statistical analysis was assessed using ANOVA followed by post hoc Pairwise Multiple Comparisons using Holm-Sidak method on SigmaPlot version 13.0. A significant difference was considered where *P* values appeared ≤ 0.05.

2.3. RESULTS AND DISCUSSION

2.3.1. Effects of SA-2 on the properties of ECs under stress conditions

Hybrid compound SA-2 decreased the production of ROS and maintained a physiologically relevant level of eNOS (**Fig. 2.2**) when evaluated in Human Umbilical Vascular Endothelial Cells (HUVECs). In this experiment, SIN-1, a pure NO donor, at a concentration of 50 μM although produced more than 90 times of NO in cell culture media (data not shown) than that of SA-2, it failed to recover intracellular eNOS levels for ECs. Additionally, the hybrid compound SA-2 at concentrations ranging from 0.05-5.0 μM effectively scavenged the excess ROS produced and maintained the redox status similar to the control (**Fig. 2.2b**), while the reference antioxidant SA-3 needed 10- to 100-fold more concentration to

achieve such effects. We also noticed that the reported NO donor antioxidant hybrid SA-5 is less effective in decreasing the ROS level.

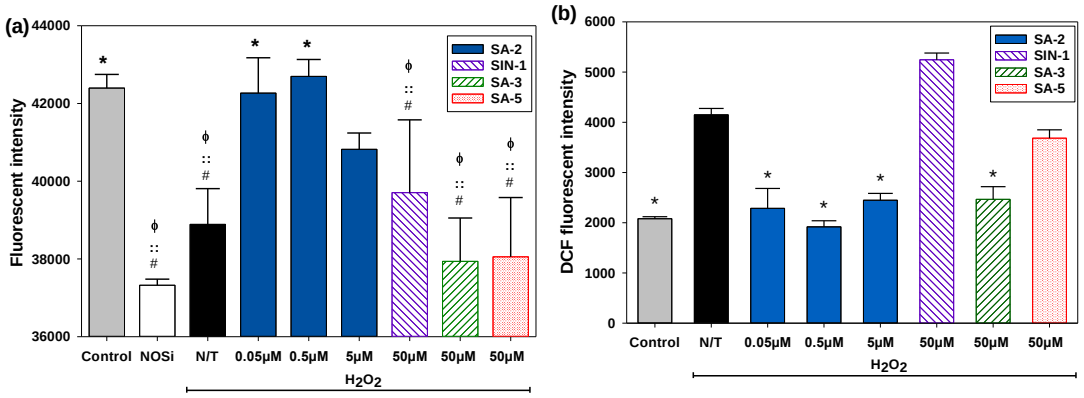

Figure 2.2. Effects of SA-2 on Nitric Oxide Synthase (NOS) activities (a) and scavenging of ROS (b) in HUVECs. After seeding and being confluent in tissue culture plates, cells were co-treated with H_2O_2 and either SA-2 at different concentrations, a reference NO donor SIN-1 (50 μM), a reference antioxidant SA-3 (50 μM) or a reference hybrid compound SA-5 (50 μM). Control samples were cells without exposure to H_2O_2 and any reagent, whereas N/T samples were cells exposed to H_2O_2 only. NOS knock-down samples (NOSi) were cells exposed to L-NNA at 50 μM as a competitive NOS inhibitor. Post 24-hour-treatment, total NOS activities (a) from treated cells was quantified using OxiSelect™ Intracellular Nitric Oxide (NO) Assay Kit where NOS activity correlates to fluorescent intensity while ROS levels (b) were quantified with DCFDA assays. Results were analyzed on SigmaPlot with ANOVA and post hoc Pairwise Multiple Comparisons using Holm-Sidak method. Data were shown as mean ± standard deviation. Stars (*), phi (ϕ), double-colon (::) and hashtag (#) indicate significant difference ($P<0.01$; $n=4$) with respect to N/T, control, SA-2 0.05 μM and SA-2 0.5 μM, respectively.

Dysfunction of ECs under oxidative stress is a major contributor of impaired vascular endothelial growth factor (VEGF) production and new vessel formation. With the ability to maintain NO and ROS at the physiological level, compound SA-2 with EC_{50} of 0.354 μM[68] protected HUVECs from H_2O_2-induced oxidative stress, demonstrating the increase in cell viability, whereas SIN-1, which produced the

elevated NO and ROS levels *in vitro*, turned out to induce more cell death (**Fig. 2.3a**).

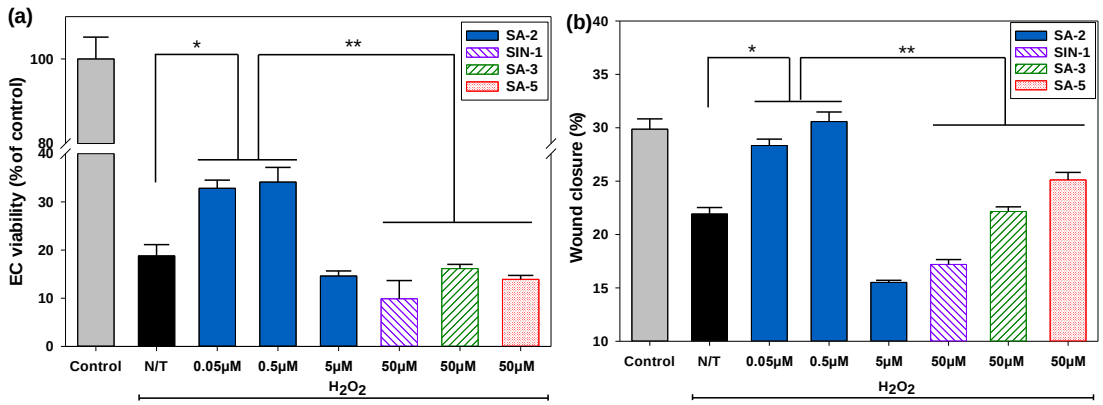

Figure 2.3. Effects of SA-2 on EC viability (a) and migration (b) under oxidative stress conditions. Cells were seeded and allowed to attach on tissue culture plates. For the cell migration study, micropipette tips were used to make scratch lines on wells, and images were taken for measuring distances of gaps. In all studies, cells were treated with H_2O_2, and SA-2 at different concentrations. A reference NO donor SIN-1 (50 μM), a reference antioxidant SA-3 (50 μM), or a reference hybrid compound SA-5 (50 μM) was added to cell samples, incubated for 24 hours, assessed for cell viability and migration, and used for comparison. Controls were cells not exposed to H_2O_2 or any treatment reagent. N/T samples were cells exposed to H_2O_2 without any test compound. Cell viability was quantified with MTS assays, while cell migration was imaged and analyzed for final distances of gaps via ImageJ. Results were then processed for statistical analysis using ANOVA followed by post-hoc comparisons (SigmaPlot). Results are presented as mean values ± SEM. Stars indicate significant differences ($P<0.05$; $n=5$) with respect to N/T (*) and reference drugs (**).

Additionally, as shown in **Fig. 2.3b**, there is good correlation between SA-2 and EC functions as shown in wound closure assessments in the migration study and the cytoprotection study of HUVECs (**Fig. 2.3a**). Namely, cells treated with a low dose of SA-2 (0.05 μM-0.5 μM) migrated similarly to the control group, while

SIN-1 showed the lowest cell migration. SA-3 and SA-5 showed an intermediate effect, but at a higher concentration (50μM).

2.3.2. Effects of SA-2 on the formation of new blood vessels

Since compound SA-2 controls the NO and ROS production and protects ECs under stress conditions, we further performed the tube formation assay to evaluate the ability of SA-2 to promote angiogenesis under an oxidative stress condition (H_2O_2). As expected, we found that, SA-2 successfully promoted new blood vessel formation (**Fig. 2.4a**) and was more efficacious than VEGF (25 ng/mL). Compound SA-2 was also found to be equally potent to GW0742 (1 μM), a peroxisome proliferator activating receptor (PPAR) β/δ agonist,[84] in inducing angiogenesis.[68]

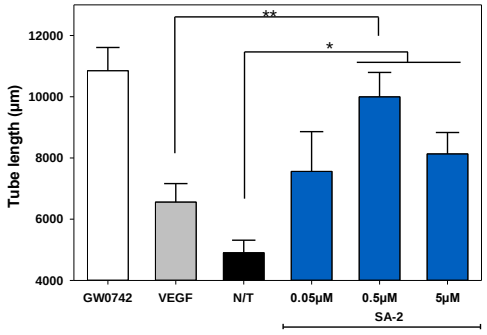

Figure 2.4. SA-2 promoted angiogenesis in ECs under an oxidative stress condition. Cells were seeded on Cultrex gel on tissue culture plates and stressed with H2O2. SA-2 at different concentrations, G0742 (1 μM), or VEGF (25 ng/mL) was added to each well. N/T samples were cells exposed to H2O2 only. After 8 hours, at least 10 images were randomly captured on a phase contrast microscope for each well (n=4 wells/sample). Images were analyzed and quantified for length of microtubes formed using ImageJ with Angiogenesis Analyzer tools. Results were then processed on SigmaPlot for statistical analysis using ANOVA followed by post hoc comparisons. Data are shown as mean values ± SEM. Stars indicate significant differences ($p<0.05$) with respect to N/T (*) and VEGF (**).

2.3.3. Effects of SA-2 on inhibiting the proliferation and migration of SMCs

In addition to increasing viability and promoting new blood vessel formation from HUVECs, hybrid compound SA-2 (0.05 µM-0.5 µM) also demonstrated substantial reduction in proliferation and migration of human aortic smooth muscle cells (HASMCs) under stress conditions (**Fig. 2.5**). Compared to the normal state, SMCs are three times more likely to grow under stress conditions (**Fig. 2.5a**). The addition of NO donor, ROS scavenger, or hybrid compounds inhibited the proliferation of SMCs at the rate of about 50%. In addition, a significant reduction in migration of SMCs was observed when cells were treated with SA-2, especially for those of lower concentrations (**Fig. 2.5b**).

Cumulatively, we observed a good correlation between the NO production, ROS scavenging, the ability to protect the HUVEC death, and migration promotion for wound healing under oxidative stress conditions by hybrid compound SA-2. The NO donor SIN-1 is previously reported to prevent EC damage due to ischemia and reperfusion[85] and attenuated SMC activation by Interferon-γ induced VCAM-1 inhibition[86] at millimolar concentrations. However, SIN-1 neither protected ECs nor promoted migration and wound closure when tested at a concentration of 50µM in our study, whereas the hybrid compound SA-2 was highly effective in a nanomolar concentration. Additionally, compound SA-2 (0.5 µM) demonstrated better potency than VEGF and was comparable to a PPAR δ/γ agonist GW0742 (1 µM) in the *in vitro* matrigel tube formation when ECs were under stress conditions. Under the same experimental condition, a pure antioxidant SA-3 or hybrid compound SA-5 were unable to protect the HUVECs from H_2O_2-induced

cell death. In SMCs, compound SA-2 (0.05-0.5μM) demonstrated superior activities in inhibiting the cell proliferation and migration under oxidative stress conditions. We have also observed that even though SIN-1 and SA-3 at concentrations of 50 μM were able to inhibit SMC proliferation, both of them did not inhibit cell migration shown as % of wound closure in **Fig. 2.5b**.

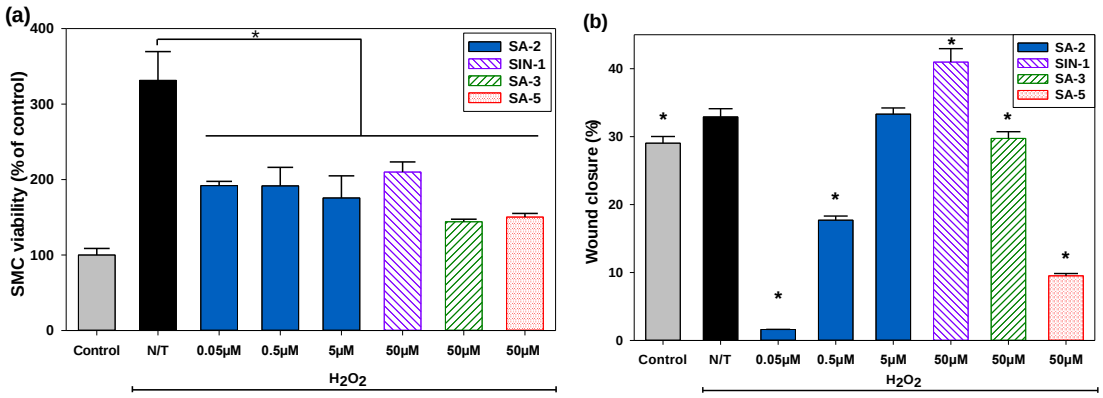

Figure 2.5. Effects of SA-2 on the SMC viability (a) and migration (b) under oxidative stress conditions. Cells were seeded and allowed to attach on tissue culture plates. For the migration study, micropipette tips were used to make scratch lines on wells, followed by washing with PBS and imaging for initial gap distances. Compound SA-2 at different concentrations, SIN-1 (50 μM), SA-3 (50 μM), or SA-5 (50 μM) was added to cell samples, stressed with H2O2 and incubated for 24 hours. Controls were cells not exposed to H_2O_2 or any treatment reagent. N/T samples were cells exposed to H_2O_2 without any test compound. Cell viability was quantified with MTS assays while cell migration was imaged and analyzed for final gap distances via ImageJ. Results were then processed on SigmaPlot for statistical analysis using ANOVA followed by post hoc comparisons. Results are presented as mean values ± SEM. Stars indicate significant differences ($P<0.05$; n=4) with respect to N/T.

Despite these exciting findings, compound SA-2 undergoes fast hydrolysis ($t_{1/2}$ less than one day at pH7.4), which is common for most of the 1,3,5-oxadiazoles containing “spontaneous” NO donating compounds.[67] To improve the therapeutic bioavailability and the aqueous chemical stability of SA-2, it was

encapsulated into FDA approved PLGA nanocarriers using a standard emulsion method similar to our previous studies.[73, 74, 79, 80] PLGA NPs have been shown to protect degradation and inactivity of various therapeutic reagents, including SA-2, and to extend the therapeutic efficacy as observed by other investigators and our group. SA-2 NPs are homogenously dispersed with an average diameter of 173±35 nm measured with a dynamic light scattering (DLS) technique. SA-2 NPs has zeta potential of these NPs was -38 ± 0.14 mV, and the NPs were stable in serum over 3 days.[68] The improvement in stability and sustained SA-2 release of drug carriers is a significant achievement to aid drug delivery to PAD patients via either intravenous (IV) or intramuscular injections.

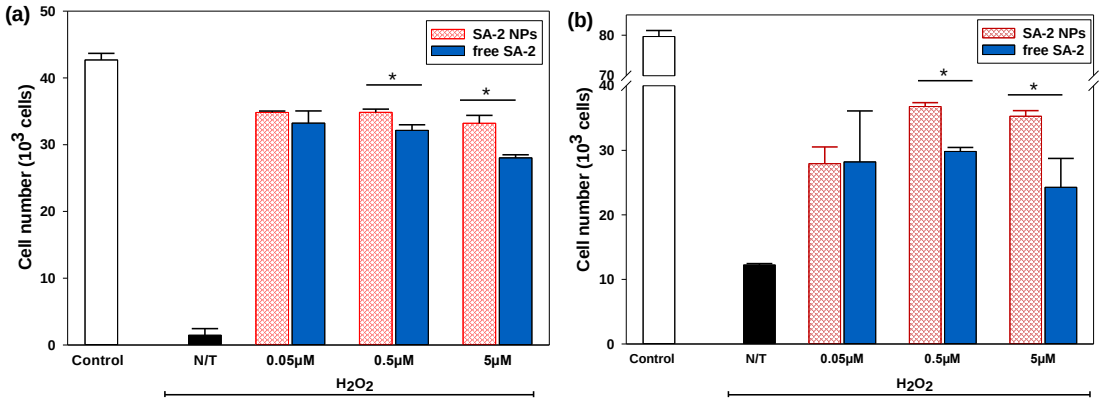

Figure 2.6. Effects of SA-2 NPs on HUVECs compared to that of free SA-2 under H_2O_2 induced oxidative stress conditions after 1 day (a) and 4 days (b) of treatment. Cells were seeded and allowed to attach on tissue culture plates. Cell samples were added to either SA-2 or SA-2 NPs at different concentrations, stressed with H_2O_2 and incubated for a predetermined treatment time (1 day or 4 days). Controls were cells not exposed to stress or any treatment reagent. N/T samples were cells exposed to H_2O_2 without any test compound. Cell numbers for studied groups were analyzed on SigmaPlot with ANOVA followed by post hoc comparisons. Results are presented as mean values ± SD. Stars (*) indicates significant differences ($P<0.05$; $n=4$) with respect to free drug at the same concentration.

Under oxidative stress conditions, SA-2 NPs at a concentration range of 0.05 µM-5.0 µM exhibited superior effects over free SA-2 by increasing ECs viability after 1 day of treatment and the effect was continued to 4 days of post treatment (**Fig. 2.6**). It is reasonable to argue that, naked SA-2 was quickly hydrolyzed in less than a day so only a portion of SA-2 took effect on EC protection, whereas NPs slowly release SA-2 to continuously induce its effects on ECs. As expected, SA-2 NPs demonstrated more effective EC protection (EC_{50} at 0.1 µM) than naked SA-2 (EC_{50} at 0.354 µM) under oxidative stress condition.

2.3.4. Effects of SA-2 NPs on angiogenesis in HUVECs

SA-2 NPs were effective in promoting *in vitro* angiogenesis similar to that of the parent drug SA-2. In the *in vitro* matrigel tube formation study, SA-2 NPs significantly promoted angiogenesis in terms of tube length under both oxidative (**Fig. 2.7a**) and hypoxic (**Fig. 2.7b**) stress conditions.

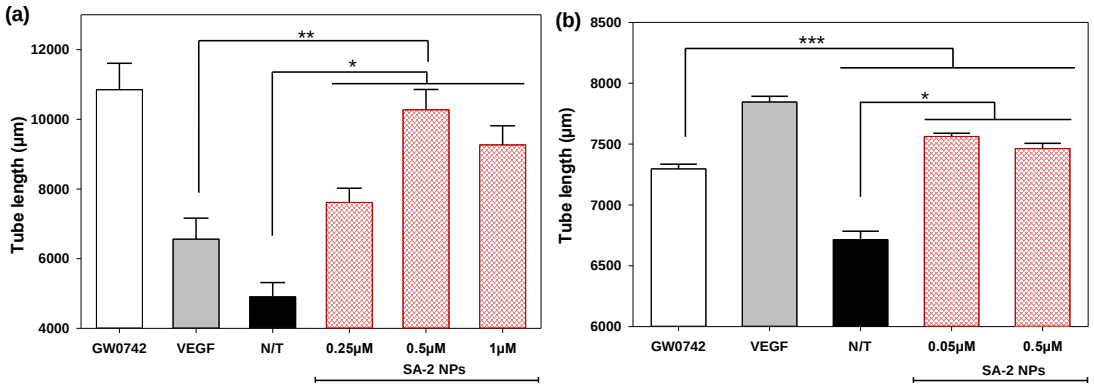

Figure 2.7. Effects of SA-2 NPs on angiogenesis of ECs under oxidative (a) and hypoxic (b) stress conditions. Cells were seeded on Cultrex gel on tissue culture plates and stressed with either H2O2 (a) or hypoxia (b). SA-2 NPs at different concentrations, GW0742 (1 µM) or VEGF (25 ng/ml), were added to each well. N/T samples were cells exposed to H2O2 only (a) or hypoxia (b) without any treatment. After 8 hours of treatment, at least 10 images were randomly

captured on a phase contrast microscope for each well. Images were analyzed and quantified for length of microtubes formed using ImageJ with Angiogenesis Analyzer tools. Numeric data were then analyzed on SigmaPlot with ANOVA followed by post hoc comparisons. Results are shown as mean values ± SEM. Stars indicate significant differences ($P<0.01$; $n=3$) with respect to N/T (*), VEGF (**) and GW0742 (***).

2.3.5. Discussion

Compounds activating the NO–cGMP pathway have been shown to be vasorelaxing, angiogenic and protective against EC dysfunction. The additional benefits on the inhibition of SMC proliferation and migration have also been reported. Comprehensive studies on soluble guanylate cyclase sGC-cGMP pathway have revealed that not only NO bioavailability is important but its concentration is also physiologically crucial. At low concentrations (nano to low micromolar), NO exhibits cytoprotection such as vasodilatation of SMCs and proliferation of ECs.[87, 88] However, higher concentrations of NO lead to reverse effects, including peroxynitrite radical formation, protein nitrosylation, and apoptosis. Hence, it is necessary to balance between superoxide and NO bioavailability at the injured arteries in order to maintain the vascular homeostasis.

Reported literature on many NO donors indicated effective concentrations in ranges from 50 to 100 µM; therefore, we chose 50 µM as a concentration for reference drugs (SIN-1, SA-3 and SA-5) in our studies. In the study by Nguyen et al.[58] a dose- and time-dependent study was performed on HUVECs, demonstrating that NO donor SIN-1 at 50 µM exhibited maximal effects on HUVEC functions. Results were quantified in terms of L-arginase activity, which contributes

crucially as a cofactor with endothelial NO synthase (eNOS) under the same low serum conditions as in our study. They also reported that although SIN-1 produced NO extracellularly, it diminished L-arginase activities and decreased endogenous NO produced by ECs.[58] In align with this study, our results observed that cells under oxidative stress conditions reduced NOS activities (thus decreased NO production) similar to that of cells treated with the NOS inhibitor (L-NNA). Additionally, SIN-1 and other reference drugs were not able to recover NOS levels to that of the control group. This might be due to mitochondria dysfunction as mentioned in literature.[59, 89] In contrast, SA-2 at 0.05 μM and 0.5 μM maintain eNOS levels equal to that of controls. As a result, EC viability, migration and angiogenesis for cells treated with SA-2 were increased while ones treated with reference drugs were not. Similar to our findings, a low dose of an NO donor DCBPY (cis-[Ru(H-dcbpy^{-})$_2$(Cl)(NO)]) to HUVECs provided NO at the same level as the control groups, and therefore induced relaxation of aortic rings and improved EC functions.[90] This result is in support of our results where SA-2 at 0.5 μM provided a physiological NO production, improved EC viability, and facilitated angiogenesis under stress conditions.

During PAD, ischemic events induce oxidative stress resulting in EC dysfunction via decreased activity of antioxidant enzymes in mitochondria. Such events of mitochondrial dysfunction and production of superoxide diminish the NO bioavailability by reacting with NO and forming toxic ONOO$^{\bullet-}$ that further damages DNA, lipids and proteins.[59] ROS and ONOO$^{\bullet-}$ specifically dysfunctionalize ECs

and increase the endo-exogenous NO imbalance. Consequently, we believe that there exists a loop where excessive NO produces more stress of ROS on ECs. Therefore, besides balancing NO levels, it is also crucial to regulate ROS levels under ischemic conditions. A study by Nguyen et al.[58] was in correlation with our study that SIN-1 elevated the ROS level in mouse aortic ECs under the stress conditions. A similar study was reported where exposure of bovine aortic endothelial cells (BAECs) to SIN-1 at 100 µM-250 µM damaged mitochondria and induced apoptosis,[89] and this effect was reversed with the help of an antioxidant diphenyl diselenide $(PhSe)_2$ at 1 µM. Other common antioxidants are TEMPOL derivatives that possess variable protection against nitration and thiol oxidation that are both induced by peroxynitrite.[91] In addition, the saturated protection (90%) and half protection (50%) were observed at 100 µM and 50 µM of TEMPO, respectively.[91] It was therefore reasonable for us to choose the concentration for antioxidant drugs SA-3 and SA-5 as 50 µM for our studies to see a maximal effect.

The idea of combining NO donor and ROS scavenging has been reported elsewhere in literature, either with physical combination or chemical (hybrid compound) combination. The former idea reported by Park et al.[92] showed that the combination of SIN-1 (100 µM) and TEMPO (100 µM) reduced pulmonary vascular resistance more than the single effect of SIN-1 (100 µM). In the same study, a similar trend was also reported for a decrease in both platelet recruitment[92] and thrombotic von Willebrand factor (an important indication in PAD) secretion. Similar to our study, Das et al.[93] investigated the effect of a cyclic hybrid compound DMPO containing $NO^{\bullet -}$ radical on regeneration of BAECs. Cells when stressed with

$ONOO^{\bullet-}$ and H_2O_2 and post-treated with DMPO showed dose- and time-dependent recovery after treatment with 50 μM of DMPO for 24 hours or 100 μM DMPO for 12 hours. In comparison, our SA-2 and SA-2 NPs are more potent and efficacious at concentrations of 0.025 μM to 0.5 μM, which are significantly lower doses. For SA-2 NPs, the protective efficacy was maintained, possibly due to the sustained NO release over a long period.

In addition to cell viability and apoptosis, the promotion of angiogenesis by antioxidants is reported by Dong et al.[94] where endothelial progenitor cells pretreated with 10 μM of commercial antioxidant FeTMPyP recovered angiogenesis at about 50%. Here we found that the hybrid compound SA-2 increased the length of tube formation from ECs nearly two-fold as compared to the non-treatment group. Compared to positive controls, our hybrid compounds demonstrated comparable angiogenic effects to that of VEGF and commercial compound GW0742.

The utilization of nanoparticles to deliver active molecules to treat PAD has been reported elsewhere in literature, by Kwon et al. for instance,[95] where poly(oxalic acid) NPs were utilized to deliver antioxidant vanillyl alcohol, and the results on HUVEC viability were dose-dependent with an increase in the NP concentrations (25 μg/mL to 100 μg/mL). This result is analogous to our results that the SA-2 NPs were more efficacious than the parent compound SA-2 on EC viability and migration at 24 hours. These results suggest that angiogenic effects *in vivo* would be improved by our SA-2 NPs, which would be investigated in the future.

2.4. SUMMARY

In summary, we have demonstrated that, the hybrid molecule SA-2 containing redox catalytic antioxidant and NO donor functionality showed better *in vitro* efficacy than a pure NO donor SIN-1, pure antioxidant SA-3 or hybrid compound SA-5. Compound SA-2 promoted angiogenesis and protected ECs against oxidative stress with EC_{50} of 0.354 μM. The hybrid compound SA-2 scavenged the ROS, inhibited SMC proliferation and migration, and promoted tube formation from ECs. PLGA NPs loading SA-2 were synthesized to protect SA-2 from spontaneous hydrolysis, a common mechanism to NO donors that is similar to S-Nitrosoglutathione (GSNO), diazonium diolates, and sydnonimines. Thus, therapeutic efficacy of SA-2 was improved in the platform of NPs. These NPs were stable in serum and provided sustained release of SA-2 over days. These SA-2 NPs were also found to be efficacious in protecting HUVECs against H_2O_2 induced oxidative stress with EC50 of 0.1 μM and more potent in promoting angiogenesis as compared to that of VEGF. To have more comprehensive investigation to this type of particles, an analog of SA-2 was further investigated for therapeutic effects both *in vitro* and *in vivo*.

CHAPTER 3. MICROBUBBLE-NANOPARTICLE CONJUGATES TO TREAT PAD

3. 1. INTRODUCTION

In chapter 2, we have demonstrated that NPs loaded with a hybrid molecule SA-2 had the ability to enhance angiogenesis and facilitate formation of new blood vessels *in vitro*. In this chapter, we investigated if microbubbles (MBs) were able to provide the controlled release of drug-loaded NPs using external ultrasound stimulation. MBs have been demonstrated to be stable and responsive to ultrasound transducer either in plain form[42, 43] and in conjugated form with NPs.[39, 40] Therefore, we hypothesized that conjugating MBs with NPs loading SA-10, an analog molecule of SA-2, would give us a drug delivery system that was controllable and provided the release of drug-loaded NPs on demand. To make the system complete, the MB-NPs were tagged with anti-mouse ICAM-1 antibodies and used on PAD mouse models through intravenous (iv) injection. The iv injection was chosen to provide medium for MB triggering the ultrasound delivery. Additionally, targeting of NPs with anti-ICAM-1 antibodies also allowed very high local accumulation of MB-NPs at the damaged muscles. It has been reported in literature that injured endothelial cells under ischemic conditions overexpressed ICAM-1 and VCAM-1.[96, 97] Having anti ICAM-1 antibodies (Abs) on MB-NPs allowed the MB-NPs to circulate and bind to endothelial cells at the ischemic limbs.

With help of external ultrasound transducers, the MBs in MB-NPs were broken and released NPs that allowed these NPs to be uptaken by the injured endothelial cells.

3. 2. MATERIALS AND METHODS

3.2.1. Synthesis of microbubbles

Microbubbles were synthesized from DPPC and DSPE at different weight ratios (6:1, 5:2, 1:1 and 2:5 w/w). For example, 6 mg of DPPC and 1 mg of DSPE were dissolved in 3 mL of chloroform for 6:1 weight ratio. The mixture was then transferred to round bottom flask that connected to rotary evaporator and run at 55^{o}C heater, 0.9mBar vacuum and 250rpm rotation for 10 minutes. Once a film was obtained, it was hydrated with 1 mL of hydration buffer (contained of v/v 5% glycerol and v/v 95% PBS), shake at 130 rpm in a shaking incubator for one hour. Next, the dissolved film was transferred to a capsule and injected with C_3F_8 gas before amalgamated at 5000 rpm in 60 seconds to form MBs. The obtained MBs were then collected and purified by adding PBS and centrifuging at 50g in 3 minutes. This process was repeated 3 times. For MBs with biotin, the same procedure was applied for DPPC and DSPE-PEG$_{1000}$-biotin.

3.2.2. Synthesis of blank and drug loaded PLGA NPs conjugating avidin

Blank PLGA and PLGA NPs loaded with SA-10 were modified with avidin through EDC/NHS chemistry. Briefly, 2.5 mg of PLGA NPs were dissolved in MES (2-(N-morpholino) ethanesulfonic acid) buffer, and 15 mg of EDC was added and

mixed well. After gentle agitating in half of an hour, 22.5 mg of NHS was added, and the suspension was shaked gently for 30 minutes. After that, 500 µg of Avidin was added and the reactant was shaked for one hour before collecting by ultracentrifugation. The washing was repeated once with PBS to remove all unreacted substances. The PLGA NP-avidin was dissolved in PBS for immediate use or lyophilized for long term storage. Fluorescent coumarin-6 loaded PLGA NPs also underwent the same procedure to obtain avidin-tagged coumarin-6 NPs, and these NPs were used to characterize the bindings with biotin-tagged MBs.

3.2.3. Synthesis of MB-NPs conjugates

After purification, MBs (synthesized from 5 mg of DPPC and 2 mg of DSPE-PEG_{1000}-biotin) were mixed with 5 mg of drug loaded PLGA NP-avidin. The mixture was gently shaked on a shaker at 50 Hz for 15-30 minutes. The mixture was purified using the same procedure to plain MBs. Next, biotinylated anti-mouse ICAM-1 Abs (abbreviated as anti-ICAM-1) were introduced to the MB-NP, shaked for 30 minutes on a shaker to allow the anti-ICAM-1 to bind to free region of avidin on NPs.

3.2.4. Ultrasound signal measurement

MBs suspended in PBS were allowed to slowly run through a ~0.03-inch diameter transparent silicon tube placed in a water bath. An ultrasound transducer was setup to have its focal point lying on the central point of the tube (as considered in cross-sectional profile of the tube). Signals of MBs in PBS, water (background) and

normal air (reference) were recorded with parameters of 1MHz frequency and 200mVpp amplitude. Final signals of MBs and air were calibrated with subtraction by the signal of water, which is considered as background of transmitting medium. The ultrasound signal stability of MBs was determined as signal amplitude of MBs versus that of a reference over time.

3.2.5. High intensity focused ultrasound (HIFU) stimulation

HIFU was applied approximately 15-30 minutes right after injection of MB-NPs. Animals were anesthetized with 2% isoflurane and placed on a holder that had a transparent window for ultrasound to go through. The animals and holder were place on a water bath that had the HIFU transducer. The animals were kept isotherm by providing heat from a heater probe. Before introducing HIFU, a thin silicon tube (0.025 inch in diameter) was applied right on top of the animal's femoral artery on the ischemic limb. Next, the ultrasound system was focused on the silicon tube, and then the focus was adjusted to lie on the animal's artery with the approximation of 0.050 inch distance from center of the tube to the center of the artery. The tubes, mimicking artery size and ultrasonic transparency, were used for determining central points, and ultrasound signals referring the medium inside the tube filling with water (background-no signal) and normal air (air signal). Once the central point of tubes was determined, the distance to move focal point was calculated as $^{0.025}/_{2}$ +0.025+ $^{0.025}/_{2}$ =0.050 inch (with the thickness of skin and

fat tissue was estimated to be 0.025 inch). The installation was briefly picturized in **Figure 3.1**.

For our preliminary data, parameters of HIFU were chosen at 15 MHz frequency, 200 mVpp amplitude and 10 ms on-duty followed by 190 ms off-duty to dissipate heat. The duty cycles were kept running in total of 15 minutes.

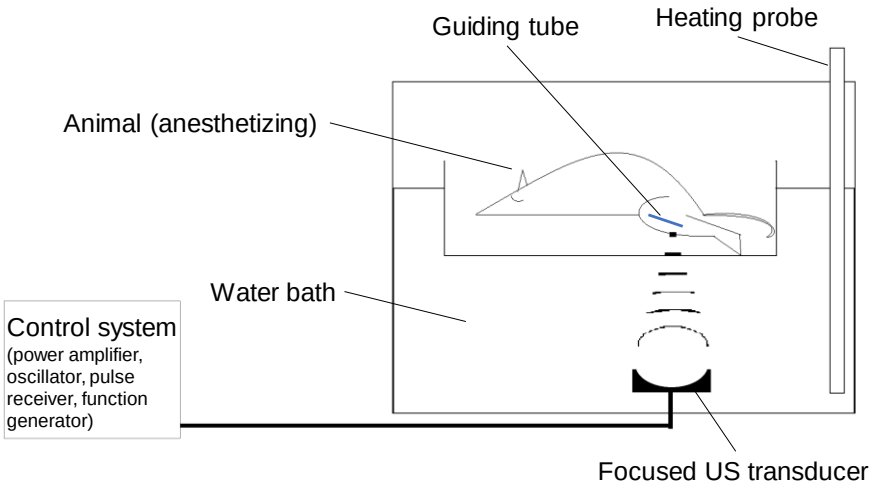

Figure 3.1. Installation of the focused ultrasound to study on PAD mice model.

3.2.1. Animal model

Since PAD happens commonly in old people, we used old mice for ischemic hindlimb animal models. To this, Balb/c mice of both sexes at age of 30-40 weeks old were chosen for our *in vivo* studies. Animals were housed in individual cage at normal diet before performing ligation. In brief, animals were anesthetized with 2% isoflurane, and prior to incision, analgesic SR Buprenorphine was injected subcutaneously (at dose of 1mg/kg for mice). Upon opening the incision on animals left legs, the membrane covering the inguinal fat tissue was carefully

separated to expose the neurovascular bundle underneath and veins and nerves were then carefully separated from arteries. Next, three pair of 1 mm-distal ties (using 6-0 or 7-0 nonabsorbable suture) followed by transection (by spring scissor) were made on femoral artery, proximal caudal femoral artery and superficial caudal epigastric artery.[98] Finally, the incision was closed by absorbable 5-0 or 6-0 sutures. The animal model should appear to be limping[99] from the time post-treatment until endpoint study. The animals were allowed to recover properly following the UTA and NIH Rodent Surgery Guidelines. All studies related to animals, including housing, surgeries, introducing materials such as nanoparticles and microbubbles, focused ultrasound, fluorescent imaging, blood perfusion analysis and treadmill running tests were conducted under the approval of UTA affiliated IACUC.

3.2.2. Therapeutic groups of study and sample size

After 3 days of ligation, mice were randomly assigned into 5 groups: Sham, MBs with HIFU, SA-10 NP-anti-mouse ICAM-1, MB-SA-10 NP-anti-mouse ICAM-1 with HIFU and MB-SA-10 NP-anti-mouse ICAM-1 without HIFU. Sham groups were injected with saline without any therapeutic treatment. The route of administration was

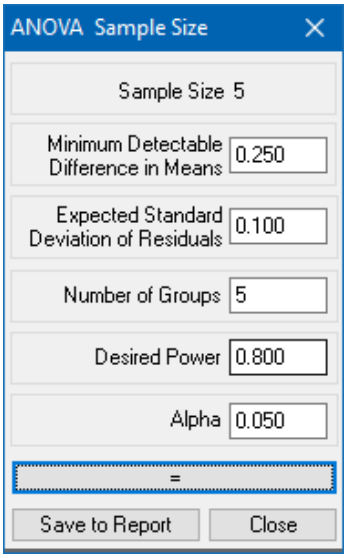

Figure 3.2. Sample size calculation for ANOVA analysis

intramuscular (IM) injection. To determine sample size, a power of analysis was processed on SigmaPlot v.13 software. Significant difference would be considered when $P<0.05$ ($\alpha<0.05$, **Fig. 3.2**). Based on our own experience and literature report, we selected power with $\alpha<0.05$ as 0.8. Calculation returned sample size as 5, or totally 25 mices were needed (**Fig. 3.2**).

3.2.3. In vivo blood perfusion and physical studies

Animals under treatments were measured for their recovery physiologically and physically. In the former study, animals were anesthetized with 1.5-2% isoflurane, and blood perfusion was measured with Laser Speckle Contrast Imaging (PeriCam PSI NR, Perimed AB). Briefly, hemoglobin in shallow vessels and capillaries responded to exciting lasers in term of color pigments. The relative blood perfusion was calculated by device software (PIMSoft), and it correlated to typical pigments. To obtain consistent and precise comparison among animals, blood perfusion indexes of each animal were obtained from ratio of relative blood perfusion of ischemic limb to that of healthy limb on the same animal. In the later study, animals after treatment were placed in individual lanes of a mice treadmill (Cat. LE8710MTS-5 lanes. Harvard Apparatus) as shown in **Figure 3.3**.

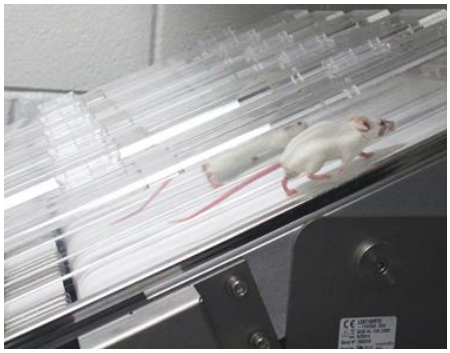

Figure 3.3. Physical recovery of mice tested on 5-lane mice treadmill. Animals were stimulated to keep running until reaching a threshold of tiredness.

The treadmill was set at 30-degree inclination. Next, the animals were then stimulated with 1.5mA electrical shocks to keep running while the treadmill speeded up as shown below:

Table 3.1. Maximal endurance protocol to test ability to walk of animals on treadmill

Start speed (cm/s)	End speed (cm/s)	Duration (mm:ss)	Stimulation (mA)	Period name
5	10	0:30	1.5	Initial speed
10	10	0:30	1.5	Stable warm up speed
10	15	0:30	1.5	Speed up 1
15	15	0:30	1.5	Stable low speed
15	20	1:00	1.5	Speed up 2
20	20	1:30	1.5	Stable high speed
20	25	1:30	1.5	Start challenge
25	25	2:00	1.5	Sign of tiredness
25	30	2:00	1.5	Challenging endurance
30	30	5:00	1.5	Endurance phase 1
30	40	2:30	1.5	Challenging
40	40	5:00	1.5	Endurance phase 2
40	50	2:30	1.5	Reaching limits
50	50	5:00	1.5	Physically endure

When the animal was not running for total of 30 seconds under stimulation, the run of animals was terminated from recording. Physical recovery of animals was then quantified as covered distance until exhaustion, which was obtained from the treadmill software.

3. 3. RESULTS AND DISCUSSION

3.3.1. Characterization of microbubbles

Microbubbles were synthesized at different w/w ratios of DPPS to DSPE. Signals of MBs at different formulations were determined over the time, and it showed that the MBs at a weight ratio 6:1 or 5:2 retained the longest US signal stability (**Fig. 3.4**). The MBs with 5:2 w/w ratio were used for later studies due to their better properties, including stability.

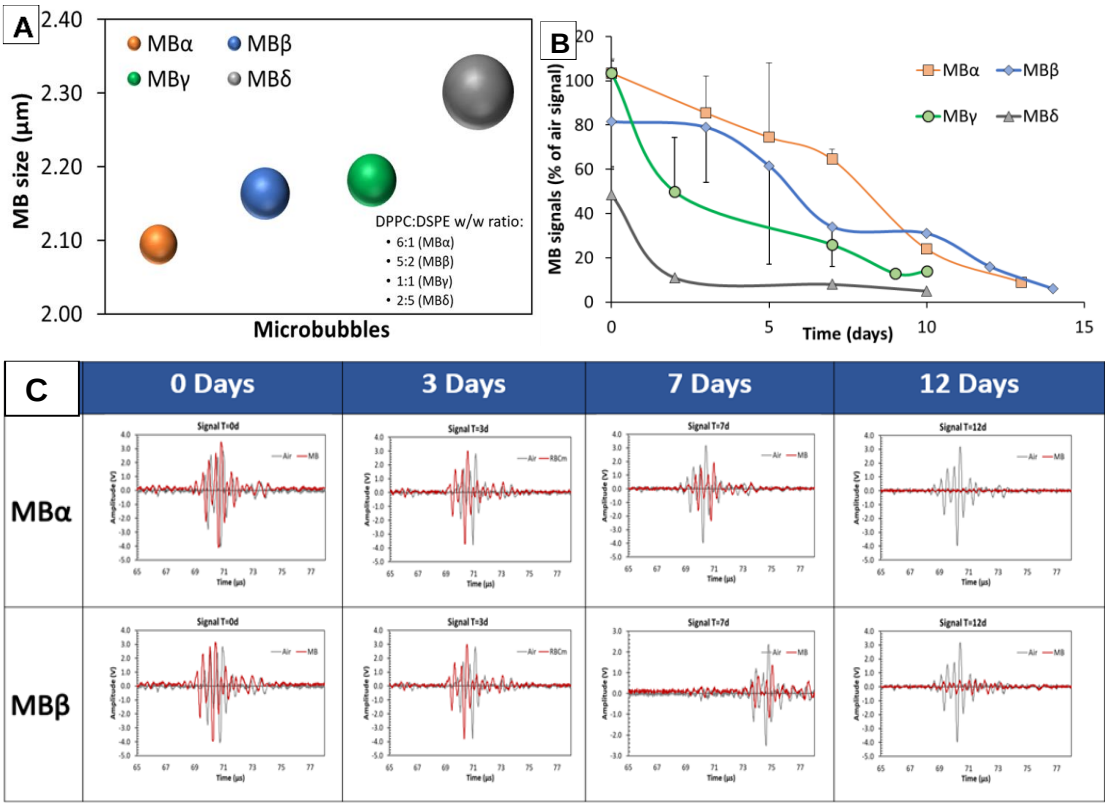

Figure 3.4. Characterization of microbubbles (A) size, (B) ultrasound signal stability and (C) representative ultrasound signals over time. Sizes of MBs were determined by dynamic light scattering (DLS) on ZetaPAL sizer (BrookHaven Instruments). Ultrasound signals of MBs and reference signals (air) were calibrated with background signals (water).

Under stimulation of HIFU at frequency of 15MHz, MBs with 5:2 (DPPC:DSPE) w/w ratio were observed to be broken due to the reduced in density and appearance of lipid debris (**Fig. 3.5**).

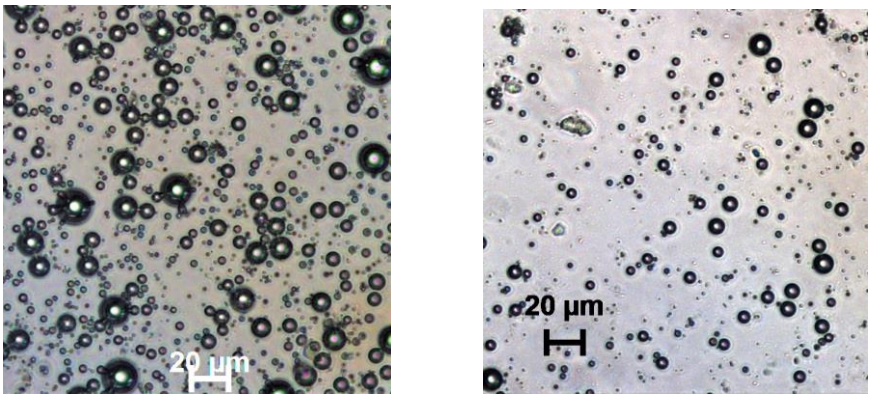

Figure 3.5. Images of MBs before (left) and after (right) introduction of HIFU. MBs were observed on white light microscope with 4X objective (40X combined) magnification.

3.3.2. Characterization of MB-NP conjugates

In order to fabricate MB-NP complexes, we chose biotin-avidin binding strategy for the fact that it was selective and among the strongest binding affinity. To do this, we synthesized MBs with biotin on the surfaces from DPPC and DSPE-PEG_{2000}-biotin following the same protocol to that of normal MBs. Meanwhile, NPs were first synthesized, and then surface-modified with avidin. The avidin on NPs not only allowed NPs to bind MBs, but also provided binding sites for conjugating with biotinylated targeting antibodies. The binding of NPs to MBs through biotin-avidin mechanism was illustrated in **Figure 3.6**.

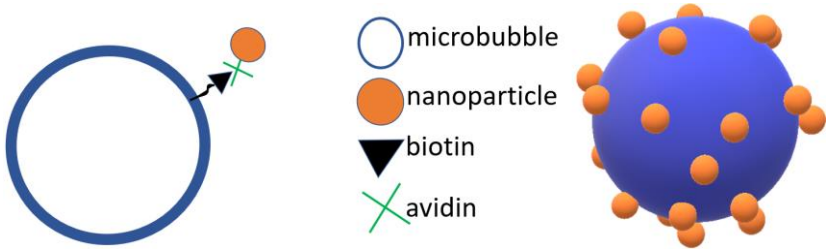

Figure 3.6. Illustration of MB-NP conjugates. Microbubbles were synthesized with biotin on surfaces. Meanwhile, nanoparticles were modified their surfaces with avidin through EDC/NHS chemistry reaction. Nanoparticles were then conjugated on microbubble surfaces through biotin-avidin bindings.

To confirmed for the appearance of biotin on MB surfaces, MBs were mixed with biotinylated FITC dyes, then the mixture was introduced with avidin and MB-biotin-avidin-biotin-FITC (denoted as MB-FITC) was formed. To get rid of unbound biotin-FITC, purification of the MBs (3 times) was performed by centrifugation at 50g in 3 minutes, where MBs formed floating layers while unbound dyes in supernatant was discarded. Finally, the dye-conjugated MBs was observed under fluorescent microscope with FITC filter. To compare, similar procedure was applied for biotin-MBs and biotinylated FITC without the addition of avidin. After purification, the MBs (denoted as plain MBs) were observed under fluorescent microscope with FITC filter. It was confirmed that MBs were tagged with biotin (**Fig. 3.7**).

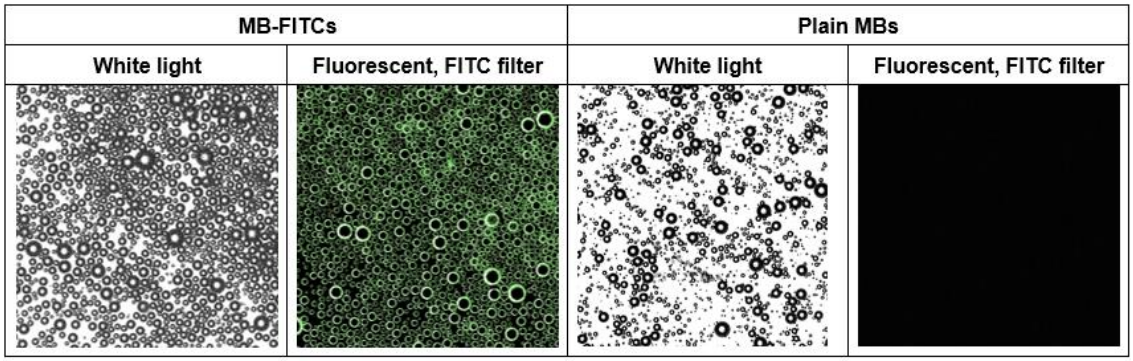

Figure 3.7. Confirmation of biotin tagged MBs. MB-biotin-avidin-biotin-FITC remained fluorescent while MBs without avidin were not able to bind FITC thus were not observed under fluorescent microscope. Pictures were captured with 10X objective magnification under white light (or bright field mode, no filter) and FITC filter (fluorescent illumination mode).

To confirm if NPs were able to bind to MBs, fluorescent NPs were utilized. Specifically, coumarin 6, a fluorescent substance having emission at 505 nm and observable with FITC filter, was loaded in PLGA NPs. The NPs, expressing green fluorescent, were modified with avidin following aforementioned procedure. Next, the coumarin 6 NP-avidin were mixed with MB-biotin, followed by centrifuging purification and finally fluorescent observation (**Fig. 3.8**). While it was obvious to observe large MBs with fluorescent corona, smaller MBs were observed with fainted small dots. However, there also appeared many bright colonies that were suspected to be NP clumps. Further purification could be the resolution to get rid of these NP clumps.

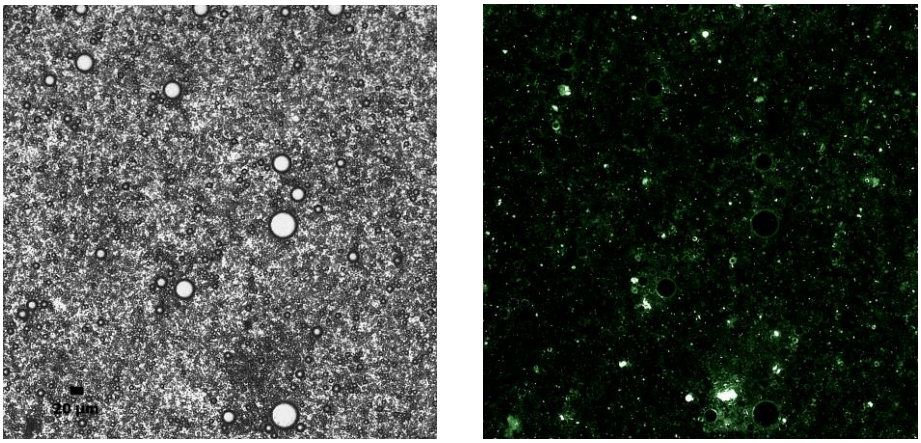

Figure 3.8. Confirmation of nanoparticles conjugating microbubbles. White light (left) and fluorescent images (right, FITC filter) of MB-NP complexes from MBs and Courmarin 6 loaded PLGA NPs. Pictures were captured with 10X objective magnification under white light (or bright field mode, no filter) and FITC filter (fluorescent illumination mode).

In parallel, measuring sizes of particles with DLS technique showed that the size changed from 2.6±0.08 µm for plain MBs to 3.1±0.14 µm for MB-NP conjugations (**Fig. 3.9**).

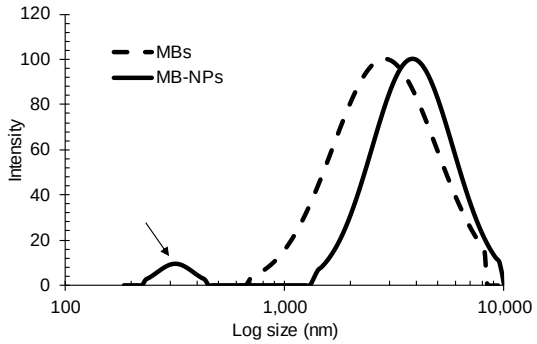

Figure 3.9. Size distribution of MBs before and after conjugation with avidin tagged NPs. Small peak (arrow) indicated small portion of NPs were not conjugated.

Conjugation efficiency was calculated from the amounts of coumarin 6 NPs before and after conjugation with MBs. Briefly, coumarin 6 NPs were dissolved in PBS and measured for fluorescent intensity in a photospectrometer. Once the NPs

were mixed with MBs, the mixture was purified via centrifugation at 50g in 3 minutes. MB-NPs were collected as a floating layer while excessive NPs stayed in supernatant. Supernatant obtained after centrifugation was measured for fluorescent intensity. Meanwhile, plain MBs were also measured fluorescent at the same excitation/emission wavelength and data was considered as a background. Fluorescent net intensity of coumarin 6 loaded MB-NPs were calibrated by subtracting background fluorescence. The amount of coumarin 6 NPs were determined from standard linear regression of a known amount of coumarin 6 NPs versus fluorescent intensity. Conjugation efficiency was calculated following equation:

$$\text{Conjugation efficiency} = \frac{NPs_{\text{in MB-NPs}}}{NPs_{\text{in MB-NPs}} + NPs_{\text{in supernatant}}} \times 100\% \qquad \text{(Equation 3.1)}$$

Using **Equation 3.1**, the conjugation of coumarin 6 NPs showed the yield of 74%.

3.3.3. Biodistribution study

Balb/c mice (both male and female) were ligated to create PAD models, rested in 3 days before randomly assigned to study groups (n=3 per group per injection). Suspension in saline of avidin-tagged ICG NPs at 4 mg/mL was prepared, then mixed with biotin-MBs for 15 minutes before adding biotinylated anti-mouse ICAM-1 antibodies and mixed for another 15 minutes, followed by centrifuging purification. Next, animals were injected total 200 µL of ICG loaded MB-NPs via IV injection through tail vein. At each time point (4, 12 and 24-hour),

animals were sacrificed; then major organs and tissues (hearts, lungs, livers, kidneys, spleens, healthy muscles and ischemic muscles) were collected and proceeded for fluorescent intensity (760/830 nm excitation/emission).

It has been shown in **Figure 3.10** that the MB-NPs bound more to ischemic limbs compared to those of normal muscles. While MB-NP complexes were shown to target to ischemic hindlimbs, it also showed that a large number of MB-NP were accumulated in spleens, livers and kidneys. MB-NPs accumulated at lung at some extents. Meanwhile, little MB-NPs were observed in hearts.

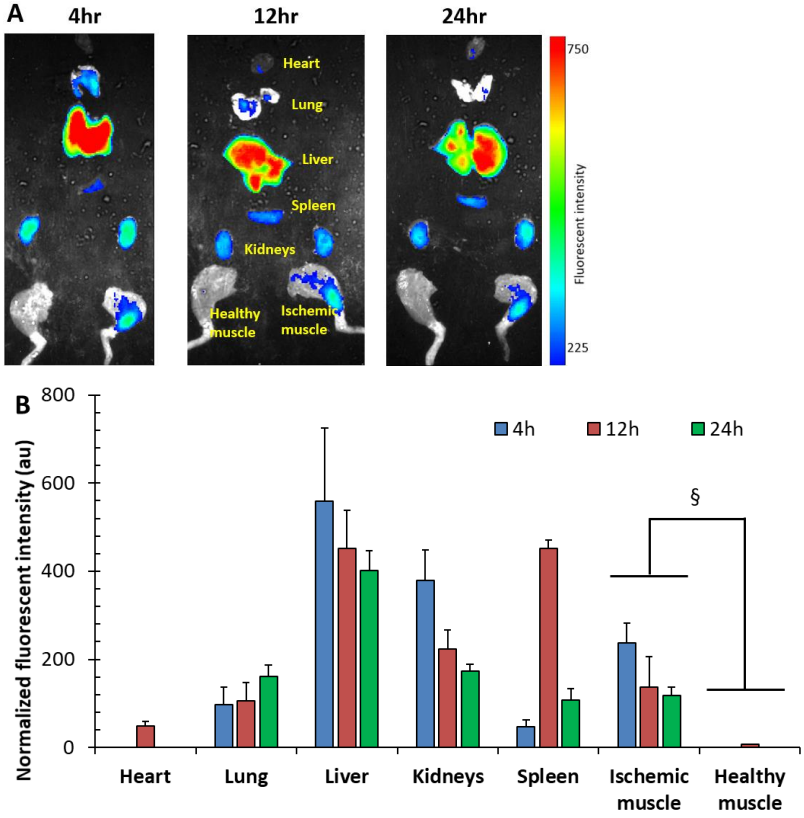

Figure 3.10. Biodistribution study of ICG loaded MB-NP-anti-mouse ICAM-1 complexes tested on PAD mouse models. (A) Fluorescent intensity of MB-NPs accumulated in tissues at different time points. (B) Quantified fluorescent intensity of MB-NPs accumulated in tissues at different time points. § indicates significant difference ($P<0.01$; $n=3$) with respect to normal muscles.

3.3.4. Blood perfusion and physical ability to walk

Here, we are presenting preliminary data on the therapeutic treatment obtaining from introduction of MB-NP conjugates and high intensity focused ultrasound. Due to the issues of facilities, animals were rested 2 weeks before the first treatment. After treatment, it shown that MB-NP with HIFU stimulation induced animal recovery in both blood perfusion and ability to walk, as significantly higher than sham group (**Fig. 3.11**). SA-10 NPs performed relatively good compared to the MB-NP with HIFU. This resulted from the fact that SA-10 NPs were tagged with anti-mouse ICAM-1; therefore, NPs were selectively bound to the injured cells at ischemic sites.

We also observed two opposite trends of data for plain microbubble treatment groups. For the physical run of animals, the microbubble-treated groups recovered quickly, in accordance with study in literature that ultrasound may mediate angiogenesis and blood supply to animals.[100] However, it showed reversely in our quantification for the blood perfusion where it slowly recovered and that was similar to sham groups. Although it showed difference in physical tests that animals treated with MB-NP complexes and with HIFU performed better than those treated with MB-NP complexes only, the results from blood perfusion did not support for the results of physical tests. Considering with results of MBs with HIFU, the therapeutic effects of HIFU was still questionable. This could be explained by the lack of optimization studies. Meanwhile, heat generated from HIFU has not been thoroughly investigated. Longer exposure of MB-NPs to HIFU might yield

more release of NPs but also might generate more heat. These issues will be investigated more profoundly in future studies. In short, the effectiveness of treatments was observed for SA-10 NPs ~ MB-SA-10 NPs with HIFU > MB-SA-10 NPs without HIFU > MBs with HIFU > Sham.

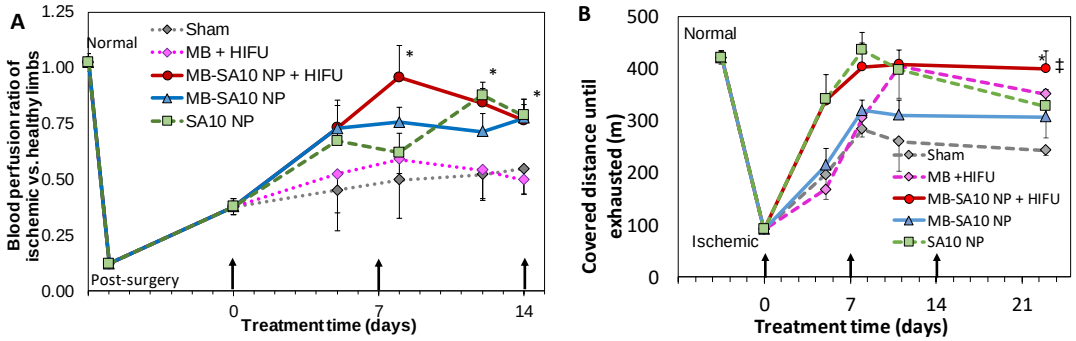

Figure 3.11. Blood perfusion indexes (A) and running test (B) of PAD models treated with MBs-SA-10 loaded NPs. Animals were dosed repeatedly every week. Animals were measured for blood perfusion on LSCI and running distance on treadmill. Data represent Mean±SEM. Data were analyzed with Welch's t-test (where equal variances not assumed) on SigmaPlot. *P<0.05 (n=5) with respect to Sham, ‡ P<0.05 (n=5) with respect to MB-NP complexes without HIFU.

3. 4. SUMMARY

In this chapter, we presented preliminary research on utilization of focused ultrasound on the control delivery of angiogenic nanoparticles. As a proof of concept, the studies revealed potential of using HIFU as a trigger method to control the delivery of NPs. We observed SA-10 NPs provided relatively equal therapeutic effects to MB-SA-10 NPs with HIFU. This result could be explained the fact that SA-10 NPs were also conjugated with anti-mouse ICAM-1 antibodies that help SA-10 NPs selectively bind to injured ECs at diseased sites. SA-10 NPs were also

dosed at a concentration that was used for conjugating with MBs. Hence, the release of SA-10 NPs from MB-NP complexes could only be low or equal to SA-10 NPs in the free form. Another explanation for low effectiveness of MB-SA-10 NPs was that an optimization study for focused ultrasound was not performed. Indeed, a set of parameters for HIFU settings were chosen; however, it might not precisely match the resolution of MBs and MB-NP complexes. Consequently, the HIFU might only effect on a small portion of MB-NP complexes. Future studies will conduct on MBs and MB-NP complexes to find out the optimizing parameters that most of the MB-NPs will undergo destruction and release NPs. A study about generating heat at different parameters will also need to be performed.

CHAPTER 4. DEVELOPMENT OF SECOND GENERATION HYBRID MOLECULE SA-10 AND ITS NANOPARTICLES

4.1. INTRODUCTION

In chapter 2, the synthesized compound SA-2 has been demonstrated to have good effects on endothelial cells *in vitro*, including cell protection, proliferation, tube formation and eNOS regulation. Although the concept of hybrid drug was proofed, it was obvious that the short half-life of SA-2 ($t_{1/2}$ less than one day at $pH_{7.4}$) limits its long-term capability. Inspired from SA-2, our collaborator Dr. Acharya has developed a new analog of SA-2, denoted as SA-10 (**Fig. 4.1**) that is better and more stable than SA-2. Besides the nitric oxide donor borrowed from SA-2, the developed antioxidant sulfate group allowed SA-10 to be more chemically stable, thus enable longer therapeutic activities. It has been reported in literature that the antioxidant activities correlate to the amount of sulfate groups of molecules.[101-103] In this chapter, SA-10 and its NPs were studied *in vitro* on endothelial cells under

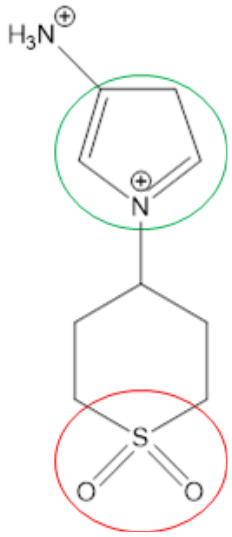

Figure 4.1. Chemical structure of SA-10 compound carrying same NO donor group (green circle) to SA-2 but upgraded antioxidant group (red circle).

stresses similar to those presented in chapter 2. Next, SA-10 and its NPs were also tested *in vivo* for their therapeutic effects on mice models.

4.2. MATERIALS AND METHODS

All other materials and processes, unless otherwise noted, were similar to those described in chapters 2 and 3.

4.2.1. Chemicals and reagents

Compound SA-10 and SA-2 were synthesized by Dr. Acharya, University of North Texas Health Science Center. Detail synthesis of SA-2 has been reported in literature previously.[67]

4.2.2. Fabrication of SA-10 NPs

SA-10 loaded PLGA NPs were prepared using the standard single emulsion technique developed in our laboratory.[72-80] In brief, 10 mg of SA-10 was dissolved 10 µL DMSO and then transferred to 3 ml of chloroform containing 90 mg of PLGA to form an oil phase. This solution was then added dropwise into 20 ml of 5% PVA solution (water phase) followed by sonication at 40W for 10 minutes to form the SA-10 loaded NPs. The emulsion was stirred overnight to completely evaporate the organic solvent. Next, the NPs were pelleted by ultracentrifugation at 25000 rpm for 30 minutes followed by washing twice with DI water. Finally, NP pellet was dissolved in DI water and lyophilized to obtain a powder form.

4.2.3. Characterization of SA-10 NPs

SA-10 NPs were characterized similarly to SA-2 NPs. Standard solutions of SA-10 were prepared, scanned and obtained absorbance values at 240 nm. From these, a linear fit was obtained to calculate loading efficiency, drug content and drug release profile of SA-10 NPs, using the **Equation 2.1**.

For the drug release study, four separate solutions at 5 mg/mL of SA-10 NPs in PBS (pH 7.4) were placed in a dialysis bag with MWCO 3.5-5 kDa (Spectrum, Catalog 131192), submerged in 20 mL PBS 1X pH 7.4 (so-called dialysate) and incubated at 37^{o}C over a time range. At each time point, 1 mL of dialysate solution was pooled and replaced with the same volume of fresh PBS. Each sampling solution was then read for its absorbance value and the amount of released SA-10 was quantified against the SA-10 standard curve. Consequently, a cumulative release profile of SA-10 over time was plotted.

4.2.4. Doses and groups of study

For comparison, the same concentrations of SA-10 (0.05 µM, 0.5 µM and 5 µM), similar to those of SA-2 reported in chapter 2, were used in our studies. For all studies unless otherwise mentioned, the no treatment group (N/T) was cells exposed to H_2O_2 only, while cells grown in complete media without exposure to anything served as a control group.

4.2.5. Cellular stress conditions

Except cell protection study where 400 µM H_2O_2 was applied in 24 hours, all other *in vitro* studies 200 µM H_2O_2 was used to avoid biased results due to the

cell death. All treatments were dissolved in low serum media (basal media with 0.2% supplement growth factors) except positive control that used complete media (basal media added 2% supplement growth factors). No treatment groups had cells exposed to stress without any treatment added.

4.2.6. Cell migration studies

Transwell chemotaxis migration studies were conducted to study effects of SA-2 and SA-10 drugs on the migration of endothelial cells under stress conditions. To this, ECs were seeded at 50,000 cells/cm^2 on upper compartment (low serum media with 200 µM H_2O_2) and attracted to migrate through 8µm-pore membrane by chemotaxis (SA compounds dissolved in low serum media with 200 µM H_2O_2) added in lower compartment. At 12 hours, migrated cells were fixed with 4% paraformaldehyde and stained with crystal violet prior to imaging and counting by Cell counter on ImageJ.

4.2.7. Cell proliferation studies

Cells were seeded at 10,000 cells/cm^2 and allowed to grow in several days. Stresses (200 µM H_2O_2) and test compound at concentration of 0.05 µM, 0.5 µM and 5 µM were refreshed every 24 hours. Cell number were quantified at day 4 using DNA assays and calculated against standard curve of DNA, which is converted to the correlated cell number.

4.2.8. In vitro angiogenesis studies

Cultrex reduced growth factor basement membrane extracted gel (Cat. 3433-005-01, R&D Systems, Inc.) was coated on bottom of µ-Slide angiogenesis wells (Cat. 81506, iBidi GmbH Co.). ECs at early passages (passage 6^{th} or earlier) were then seeded on gel at a seeding density of 25,000 cells/cm^2. Next, cells were treated with treatment groups (SA-2, SA-10, SA-10 NPs, VEGF) under stress condition (200 µM H_2O_2). After 12 hours of incubation, formation of new microtubes were visualized and captured on phase contrast microscopes. Images were then stacked and processed with Angiogenesis analyzer on ImageJ.

4.2.9. Tissue histology

At endpoint, animals were euthanized and gastrocnemius tissues of the ischemic hindlimbs were collected. The tissues were fixed with 4% paraformaldehyde overnight, then saturated with 30% sucrose solution before undergoing cryo-sectioning. For cryo-sectioning, tissues were placed upright in a mold and filled with optimized cryo temperature solution (OCT, Fisher Scientific, Catalog 23-730-571). Once tissues were frozen at -80^{o}C, the tissues were sectioned in cross sections on a cryosectioning machine with thickness of 6 µm. The distance between sections of the same tissues were 18 µm. The sections were then stained with Hematoxylin & Eosin following manufacturer's protocol. Finally, the stained tissues were observed and captured images on a microscope.

4.2.10. Therapeutic groups of study and sample size

After 3 days of ligation, mice were randomly assigned into 4 groups: Sham, free SA-10, SA-10 NPs and blank PLGA NPs. Sham groups were injected with saline without any therapeutic treatment. Based on study of biodistribution, the route of administration was intramuscular (IM) injection. To determine sample size, a power of analysis was processed on SigmaPlot v.13 software. Similar parameters to those in chapter 3 were selected. Calculation yielded sample size as 5, or totally 20 mices were needed.

4.2.11. In vivo blood perfusion and physical test

Animals under treatments were measured for their recovery physiologically and physically following the same procedure as described in chapter 3.

4.2.12. Statistical analysis

All the experiments were performed with n = 3÷6. Data were expressed as mean ± SEM. The statistical analysis was assessed using ANOVA followed by post hoc Pairwise Multiple Comparisons using Holm-Sidak method on SigmaPlot version 13.0. A significant difference was considered where *P* values appeared ≤ 0.05.

4.3. *IN VITRO* RESULTS AND DISCUSSION

4.3.1. Effects of SA-10 free drug to EC functions in comparison to SA-2

The new drug SA-10 was tested for its abilities to protect ECs. Unlike SA-2 that had a narrow effective range of concentration up to 1 µM, SA-10 provided a

wider range up to 100 µM (**Fig. 4.2A**), exhibiting that our new hybrid compound was more potent than the previous published drug SA-2.[68] The EC functions on regulating eNOS were also studied by SA-2 and SA-10, and it showed that both drugs were successfully maintained EC viability and induced eNOS signals under stress conditions (**Fig. 4.2B**).

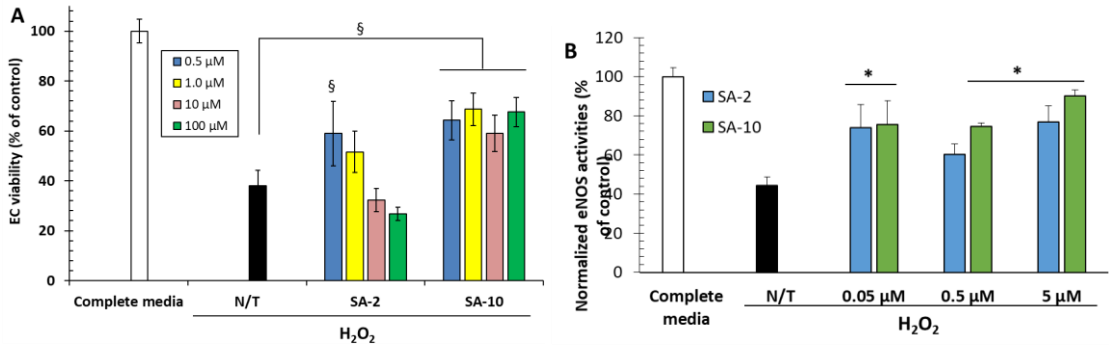

Figure 4.2. Effects of SA-10 on the viability and eNOS production of ECs under stress conditions. A) Cell protection study. HUVECs were seeded 10,000 cells/cm^2 and treated with SA-2 and SA-10 at various concentrations. Except positive control group where cells exposed to complete media and no stress, all other groups had cells in low serum media with 400 µM H_2O_2; N/T groups are no treatment groups (cells without any therapeutic agent added). B) Endothelial NO synthase enzymatic activity study. Cells were treated similar to cell protection study. After treated with SA-2 or SA-10 at different concentrations under stress conditions, cells were exposed to nitric oxide probes of the Oxiselect^{TM} intracellular eNOS quantification kit, and the reading fluorescent correlated to the activities of eNOS. Data presented as mean±SD converted versus control groups. * and § indicate significant difference ($P<0.05$ and $P<0.01$, respectively, n=4) compared to N/T.

4.3.2. Effects of SA-10 loaded NPs on EC functions

SA-10 was further tested on ECs to evaluate if it enhanced the responses of EC under stress conditions. First, a longer protection study was performed (**Fig. 4.3A**) and it showed that ECs were protected over the course of 2-day stress with

400 µM H_2O_2. A further study on proliferation of ECs were performed over the course of 4 days, and it was obvious that ECs were enhanced their proliferation under stress conditions by SA-10 (**Fig. 4.3B**). SA-10 also performed comparably to SA-2 in term of induce EC migration at a concentration equal to the optimal concentration of SA-2 (**Fig. 4.3C**). As ECs were proved to be induced their viability, migration and proliferation, it was important to study if ECs were able to form new blood vessels. This process was investigated using a 2D culture in angiogenesis study, quantifying for the formation of new microtubes. Interestingly, SA-10 significantly induced tube formation by ECs under stress conditions. This was significantly higher than that of no treatment group and comparable to free VEGF under stress and healthy cells under no stress (**Fig. 4.3D**).

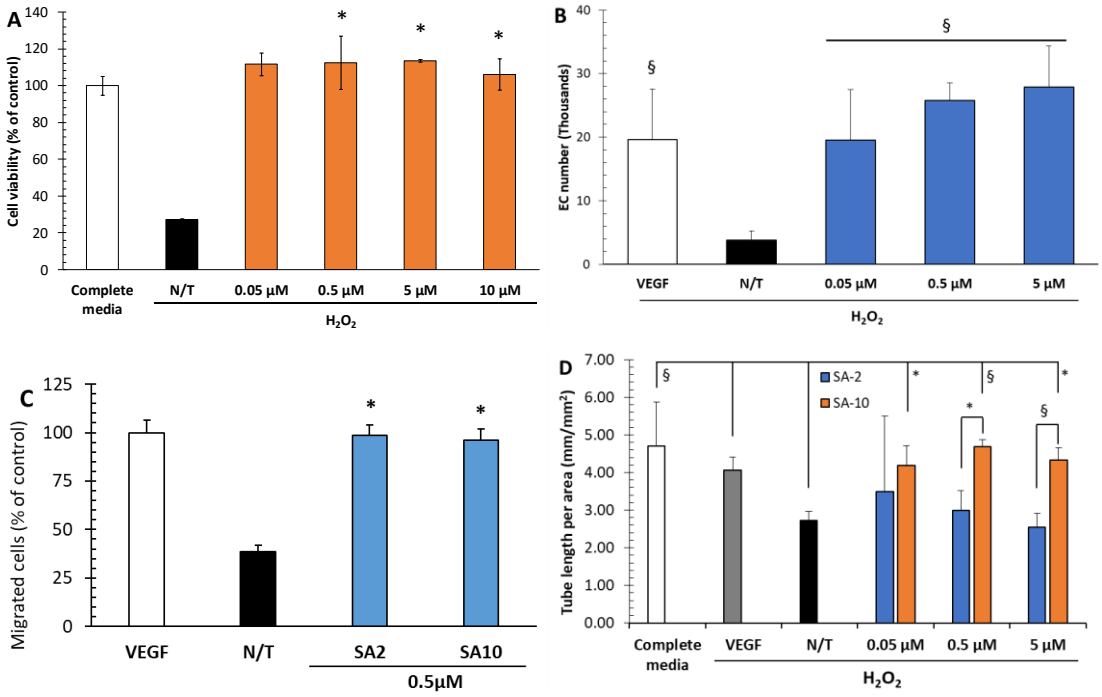

Figure 4.3. Effects of SA-10 on EC functions under stress conditions. **A**) Cell protection. Cells were seeded at 10,000 cells/cm^2, treated by different doses of test compounds under stresses

over 2 days, and the cell viability was quantified by MTS assays. Bar height represents Mean±SD. **B**) Cell proliferation. Cells were seeded at 10,000 cells/cm^2. Stresses and test compounds were refreshed every 24 hours. Cell number were quantified at day 4 using DNA assays and calculated against standard curves of DNA vs cell number. Data represented as Mean±SD. **C**) Cell migration via transwell assays. Cells were seeded at 50,000 cells/cm^2 on upper compartment and attracted to migrate through 8µm-pore membrane by chemotaxis added in the lower compartment. At 12 hours, migrated cells were fixed with 4% paraformaldehyde and stained with crystal violet prior to imaging and counting by Cell counter on ImageJ. Data represented as Mean±SD. **D**) Microtube formation. Cell were seeded 25,000 cells/cm^2 on matrigel under stress and SA treatments. Formation of microtubes was captured at 12 hours and analyzed by Angiogenesis analyzer on ImageJ. Data represented as Mean±SEM. Control: Cells in complete media (2% supplement growth factors); N/T: Cells in low serum (0.2% supplement growth factors and without any SA-2 or SA-10) with H_2O_2 200 µM. Treatment groups: Drug dissolved in low serum media. § and * indicated significant difference with respect No treatment (N/T) where $P<0.01$ and 0.05, respectively.

SA-10 has proved its potency in protecting endothelial cells, inducing proliferation and forming of new blood vessels in vitro, it was needed to package in nanoparticles to provide longer therapeutic efficacy and a controlled delivery lately. SA-10 was loaded in PLGA NPs similar to that of SA-2 loaded PLGA NPs. The PLGA NPs had the drug content of 25 µg SA-10 per mg of NPs. A drug release profile was plotted, giving a biphasic release where 30% of drugs was released in the burst phase while a sustained release of drugs was observed up to 80% at 5 days (**Fig 4.4A**). Migration study also showed that SA-10 loaded PLGA NPs facilitated EC migration. The highest effect was obtained at a concentration of 25 µg/mL (**Fig. 4.4 B&C**).

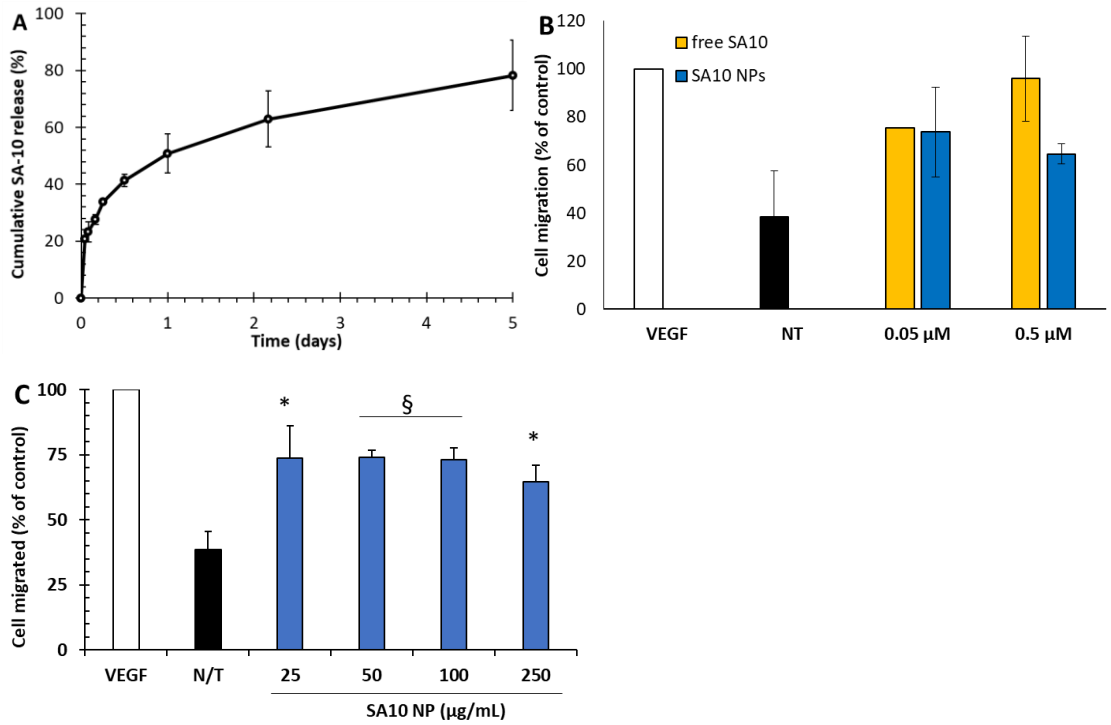

Figure 4.4. Effects of SA-10 NPs on ECs. **A**) Release profile of SA-10 loaded PLGA NPs. **B**) Transwell chemotaxis migration study of cells under treatment of SA-10 and SA-10 NPs. The amount of SA-10 NPs was back-calculated from release profile and drug content to have SA-10 released at 12 hours equal to that amount of free SA-10. All groups were subject to 200 µM H_2O_2 stress, and all treatment substances were dissolved in low serum media. Study was spanned in 24 hours. Migrated cells were fixed and stained with crystal violet before counted with imageJ. **C**) Transwell chemotaxis migration study of cells under treatment of SA-10 NPs at different concentrations. The study settings and conditions were unchanged from previous studies. Data represented as Mean±SD. Control: Cells in complete media (2% supplement); N/T: Cells in low serum (0.2% supplement) with H_2O_2 200 µM. Treatment groups: SA-10 or SA-10 NPs dissolved in low serum media.

4.4. *IN VIVO* RESULTS AND DISCUSSION

4.5.1. Biodistribution study

Before testing with therapeutic agents, animals were undergone biodistribution study to confirm for the best administrative route (**Fig. 4.5**).

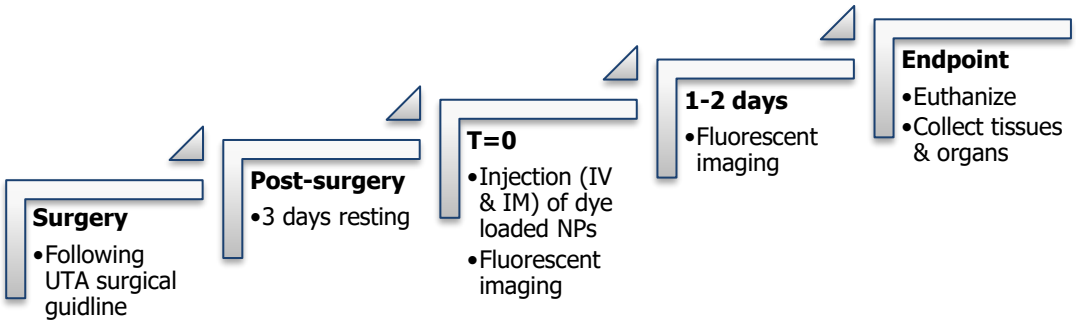

Figure 4.5. Flow chart of biodistribution study.

Balb/c mice (both male and female) were ligated to create PAD models, rested in 3 days before randomly assigned to study groups (n=3 per group per injection). Next, animals were injected total 100 µL of ICG nanoparticles suspension in saline at 4 mg/mL (16 mg/kg) via either IM (4 injections 25 µL each) or IV (one injection through tail vein) administrative route. At each time point (0, 24 and 48-hour), animals were sacrificed, and major organs and tissues (hearts, lungs, livers, kidneys, spleens, healthy muscles and ischemic muscles) were collected and proceeded for fluorescent intensity measurements. In parallel, PAD animals without any injected dye were sacrificed, and tissues were collected and imaged for background signals.

Figure 4.6A clearly showed that, through IM injection, the vast majority of NPs localized in the muscles while small amount of NPs localized in other organs. The amount of NPs localized at the hindlimb muscles was significantly higher in the IM injection compared to that of IV injection. Moreover, the IV injection had particles deposited more at major organs such as livers and kidneys (**Fig. 4.6B**).

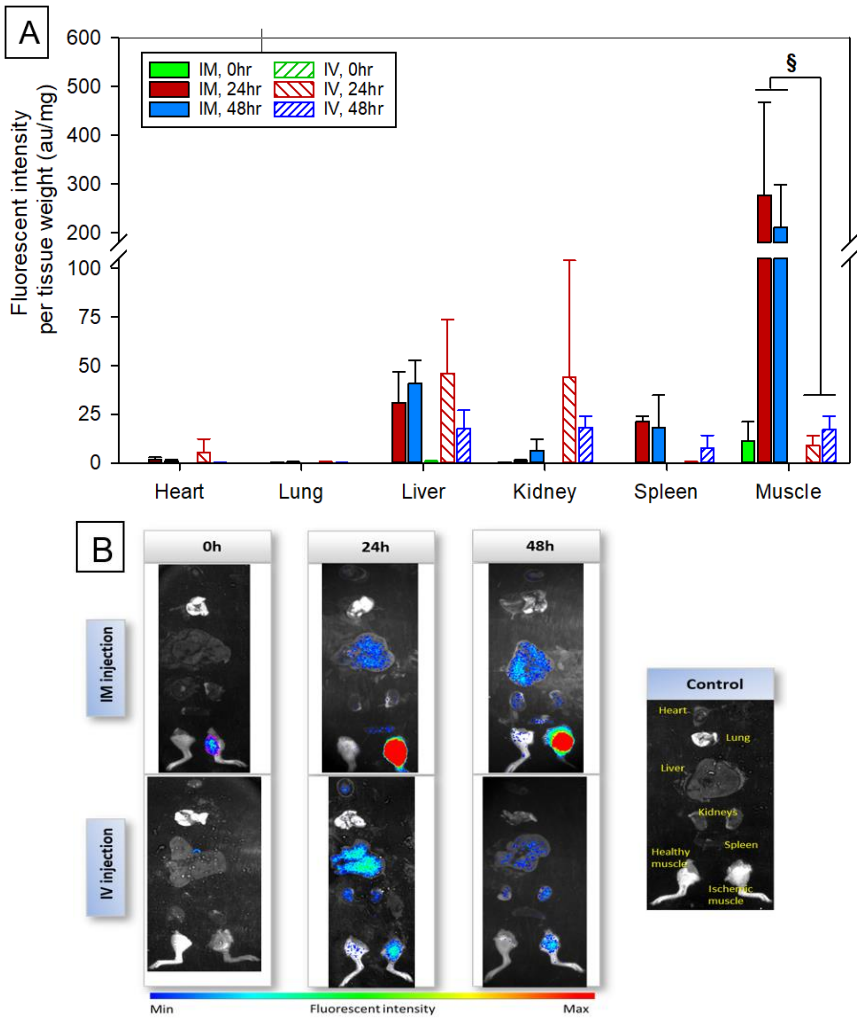

Figure 4.6. Biodistribution study of ICG-loaded PLGA nanoparticles through intravenous (IV) and intramuscular (IM) injections. **A**) Fluorescent intensity of collected tissues and organs at different time points; **B**) Quantified of dye NPs accumulated in tissues and organs at different time points. Data presented as Mean±SD. Student's and Welch's t-test were run and § indicated significant difference ($P<0.01$) with respect to IV injection.

Another pilot study was also performed using DiD loaded PLGA NPs over 6 days. The quantification of live fluorescent imaging (**Fig. 4.7**) demonstrated a long retention of particles at the muscles. The amount of particles stayed highest up to 2 days, then gradually decrease due to the dye release and cleared from bodies.

Therefore, it affirmed that IM administration was the best route to study for therapeutic efficacy of SA-10 loaded NPs.

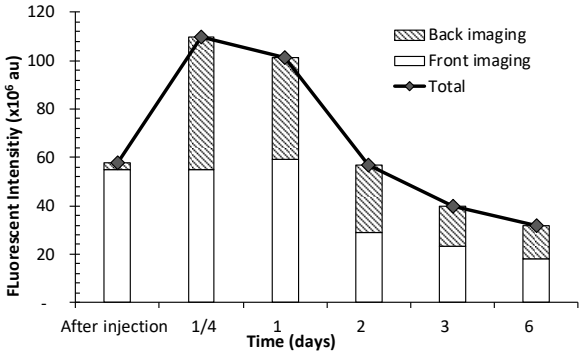

Figure 4.7. Retention of DiD loaded PLGA NPs at injection site via IM administration over 6 days of study. Animals were captured real-time fluorescent images at dorsal and ventral positions (front and back imaging, respectively).

4.5.2. Animal study design

Since SA-10 and SA-10 loaded PLGA NPs expressed good effects on ECs, the free drug and drug loaded NPs were therefore undergone animal studies to test for their therapeutic effects *in vivo*. **Figure 4.8** showed the study design for our treatment plan. Briefly, animals were undergone surgery to create PAD model as mentioned in Materials & Methods sections. After 3-day period of resting and monitoring, animals were subjected to treatment of either drug-loaded particles or free drugs. All materials were dissolved in sterile saline and administered through intramuscular (IM) injection. At predetermined timepoints, animals were measured blood perfusion indexes and perform running tests. At the endpoint, animals were euthanized and collected tissues to perform immunohistology.

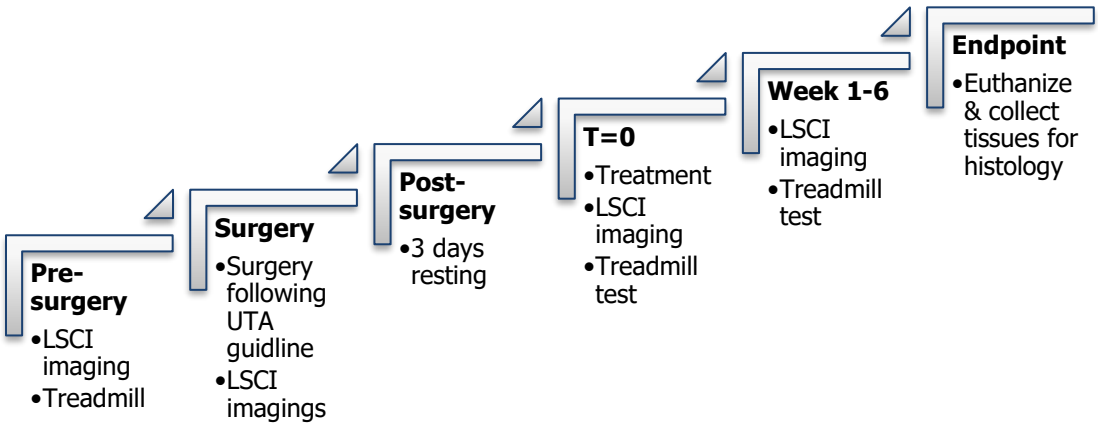

Figure 4.8. Schematic study design for treatment on PAD models.

4.5.3. Dose dependent therapeutic effects in vivo

Several doses of SA-10 loaded NPs were used to test for recovery of animals in PAD events. The pilot study showed that most of the treatment groups improved blood supply for animals (**Fig. 4.9**).

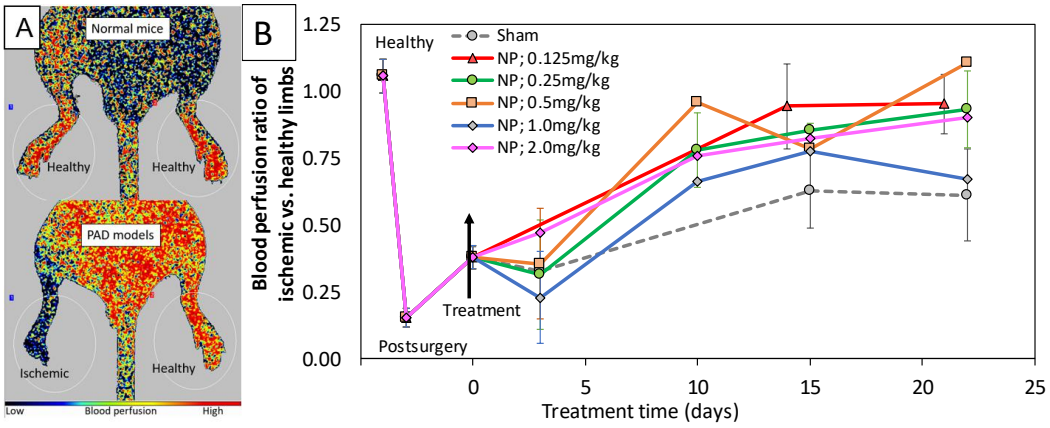

Figure 4.9. Effective doses of SA-10 NPs on salvaging limbs in animals. **A**) Blood perfusion images of animal with Laser Speckle Contrast Imaging (LSCI): More blue color indicated less blood supply while more red color indicated more blood supply. **B**) Blood perfusion ratio of ischemic limb vs uninjured limb of the same animal. Animals was injected once through IM administration. Sham was injected with saline only while (n=3÷5)

The NPs at doses 0.125 mg/kg and 0.25 mg/kg consistently improved the treatment over the time while higher doses fluctuated. It might be possible that higher doses (>1 mg/kg) toxicated the animals. Therefore, a lower but effective dose of 0.125 mg/kg was chosen for more comprehensive investigation in later studies.

4.5.4. Physiological and physical recovery

In this study, animals were dosed twice at time zero and 7th day. Since animals were treated with NPs and free drug, the drug may be cleared out from bodies. We wanted to see the effects of the drug itself, so the animals were dosed at day 7 (all types of treatment materials) to attenuate the drug clearance. After that, the animals were not be repeated the treatment since we would like to monitor the advances of SA-10 loaded NPs against the free SA-10.

As shown in **Figure 4.10**, the SA-10 NPs performed better than sham and blank vehicles either in term of blood perfusion indexes or endurance run. Free drug performed better than sham and blank vehicle at the beginning when animals were repeated the doses; however, as animals were not given another dose, the recovery was decreased. Meanwhile, the NPs, given by biodistribution study that they stayed long in the muscles, sustained release SA-10 and provided therapeutic effects to the animals.

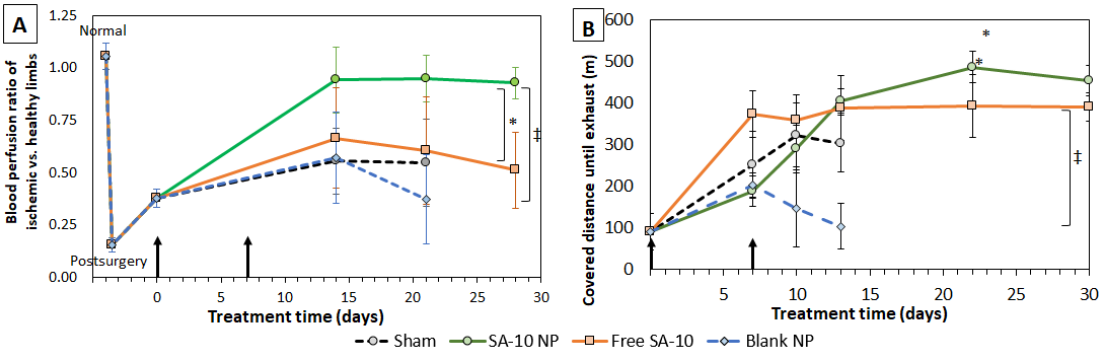

Figure 4.10. Physiological (A) and physical (B) recovery of PAD models under treatment of free SA-10 and SA-10 loaded PLGA NPs. Animals were ligated to be PAD model, rested in three days before randomly assigned into treatment groups. Free drug and NPs were dosed to have the same amount drug of 0.125 mg/kg. Blank vehicles were injected at the same amount to that of SA-10 NPs (16 mg/kg). Sham group was treated with saline only. All treatments were administered via IM injection. The treatments were applied on day 0 and day 7 (Vertical arrows). Blood perfusion was measured on Laser Speckle Contrast Imaging and quantified as ratio of blood indexes on ischemic versus normal limbs of the same animal. Exhaustion test was quantified as ability of animal to walk (in distance length) on treadmill until the animals exhausted. * and ‡ indicated significant difference ($P<0.05$; $n=5$) versus Sham and blank vehicles, respectively.

4.5.5. Tissue histology

After 4 weeks, animals were euthanized, and tissues were collected. Tissues were stained and observed for new vessel formation. Sections were observed for the formation of new blood vessels in both fat tissues (**Fig 4.11A-C**) and muscles (**Fig. 4.11D-F**). It has been shown that, although sham groups showed visibility of arteries and veins, there was little sign of red blood cells compared to other groups. This could be considered that the vessels were pre-existed vessels instead of newly created ones. The large vessels in **Figure 4.11B** (~100 µm) might be pre-existed; however, the small one and the high amount of

red blood cells could be explained by the formation of connected microvessels elsewhere. The small vessels (**Figures 4.11B&C**) were considered as newly formed due to the thin walls. In muscles, the same trend was observed. More interestingly, more sprouting endothelial cells (yellow arrows) were observed in **Figures 4.11E&F**, indicating that SA-10 and SA-10 NPs induced angiogenesis more than that of sham groups.

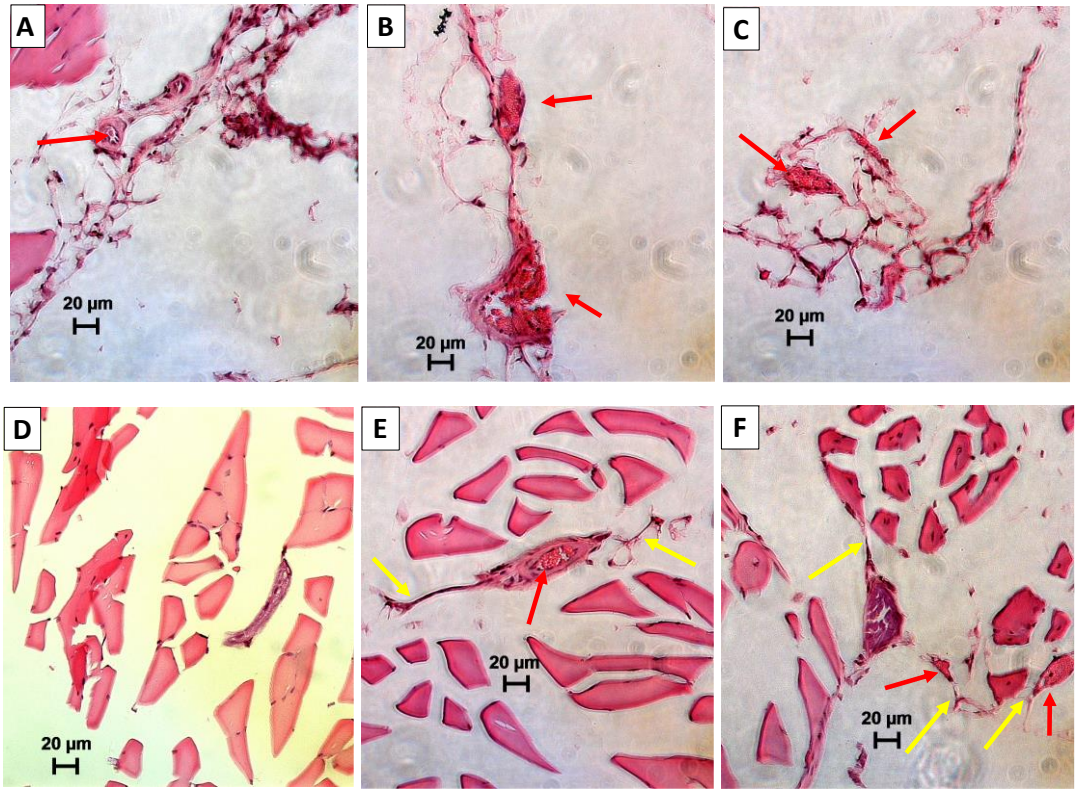

Figure 4.11. Representative images on the formation of new blood vessels of Sham (A, D), free SA-10-treated (B, E) and SA-10 NP-treated (C, F) groups. Slices obtained from ischemic gastrocnemius with OCT cross-sectioning and H&E staining. (A-C) new blood vessels formed in fat tissues; (D-F) new blood vessels formed in muscles. Red arrow: Appearance of red blood cells (stained in light red spherical with no appearance of nucleus); Yellow arrow: Sprouting endothelial cells.

Lastly, taking investigation into pre-existed major arteries, it was shown that many capillaries were formed on the current structures with help of SA-10 and SA-10 NPs (**Fig. 4.12**). Interestingly, the sham groups consisted of thinner blood vessel walls compared to that of SA-10 and SA-10 NPs. This could be explained by the fact that endothelial cells were starved and were eradicated from the vessel walls in the sham groups while in the treatment groups, cells were supplied with blood at some extents, due to formation of new vessels (black arrows). Red blood cells were also observed (yellow arrows, **Fig. 4.12C**) in the arteries of animals treated with SA-10 loaded PLGA NPs.

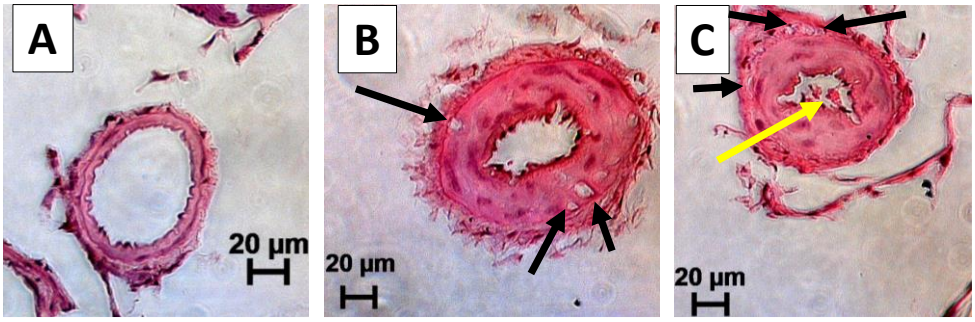

Figure 4.12. New capillaries (black arrows) formed on current arteries in sham (A), SA-10-treated (B) and SA-10 NP-treated (C) groups. Yellow arrow: Red blood cells. H&E staining.

4.5. SUMMARY

In this chapter, we have investigated a new synthesized hybrid drug SA-10. The outcome was better than the published compound, SA-2. Moreover, the outcomes matched our hypothesis that the combination of NO donors and antioxidants help recovered animals from ischemic injuries. It was also supported that the NPs helped to protect the drug and to prolong its therapeutic effects *in vivo*.

CHAPTER 5. SUMMARY, LIMITATIONS, AND FUTURE STUDIES

In previous chapters, the angiogenic nanoparticles were introduced and tested *in vitro* and *in vivo*. Promising results were obtained with SA-10 NPs, showing that the angiogenic NPs protected the therapeutic molecule SA-10, slowly released to regulate nitric oxide and reactive oxygen species that eventually promoted the formation of new blood vessels. Animals treated with free SA-10 and SA-10 loaded PLGA NPs showed an enhancement in angiogenesis. Blood perfusion indexes and the ability to walk of animals were also recovered in hindlimb mice. In short, the animals were cured at some extents. Meanwhile, microbubbles were synthesized, characterized and showed proof of concept that MBs could be incorporated with angiogenic particles, be broken on-demand with the stimulation of high intensity focused ultrasound. However, *in vivo* studies on PAD mice models with MB-conjugating SA-10 NPs exhibited a similar trend with that of SA-10 NPs.

Although promising results were obtained preliminarily, there had been many limitations needed to be solved in the future. Firstly, an optimization of HIFU were conducted to find out the optimal parameters such as frequency, intensity, duty circle, and so on. The optimal parameters should yield high percentage ablation of MB-NPs with minimum heat production. The ablation testing was conducted on either phantom system or *ex vivo* (for instance mice femoral arteries, pig hearts or chicken breasts). Second, a study on the heating by HIFU were conducted. It is crucial that the heat should not exceed survival threshold of endothelial cells and living tissues. More in-depth studies of HIFU should be

performed. Finally, the stability of MBs and MB-NP conjugates are quite low regarding with the requirement of translation studies. Several methods to prolong signal stability of MBs should be studied to make it feasible storing MBs for a long-term storage and usage.

APPENDIX

ABBREVIATION

ABI	Ankle-brachial index or Ankle-brachial pressure index
ALI	Acute limb ischemia
bFGF	Basic fibroblast growth factor
CLI	Critical limb ischemia
CVD	Cardiovascular disease
DPPC	Dipalmitoylphosphatidylcholine
DSPE	Distearoylphosphatidylethanolamine
EC	Endothelial cell
EC_{50}	Effective concentration (Concentration of drug that 50% of cells were recovered compared to the maximum recovery cells)
eNOS	Endothelial Nitric oxide synthase
CTA	Computed tomography angiography
MRA:	Magnetic resonance angiograph;
GDMT	Guideline-directed management and therapy
FUS	Focus ultrasound
HDF	Human dermal fibroblast cell
HDFm	Human dermal fibroblast cell membrane
HGF	Hepatocyte growth factor

HIFU	High intensity focused ultrasound
HUVECs	Human umbilical vascular endothelial cells
iPSC-ECs	induced pluripotent stem cells promote angiogenesis
MB	Microbubble
MB-NP	Microbubble nanoparticle conjugates
MSC	Mesenchymal stem cell
MSCm	Mesenchymal stem cell membrane
NGF	Nerve growth factor
NO	Nitric oxide
NP-avidin	Nanoparticle surfaced modified with Avidin
PAD	Peripheral Arterial Disease
RBC	Red blood cell
ROS	Reactive oxygen species
SMC	Smooth muscle cell
SPP	skin perfusion pressure
$TcPO_2$	Transcutaneous oxygen pressure
TP	Toe pressure
VEGF	Vascular endothelial growth factor

REFERENCES

1. Dua, A. & Lee, C.J. Epidemiology of Peripheral Arterial Disease and Critical Limb Ischemia. *Techniques in Vascular and Interventional Radiology* **19**, 91-95 (2016).
2. Dua, A. et al. Preventable Complications Driving Rising Costs in Management of Patients with Critical Limb Ischemia. *Ann. Vasc. Surg.* **33**, 144-148 (2016).
3. Go, A.S. et al. Heart disease and stroke statistics--2014 update: a report from the American Heart Association. *Circulation* **129**, e28-e292 (2014).
4. Gerhard-Herman, M.D. et al. 2016 AHA/ACC Guideline on the Management of Patients With Lower Extremity Peripheral Artery Disease: Executive Summary: A Report of the American College of Cardiology/American Heart Association Task Force on Clinical Practice Guidelines. **135**, e686-e725 (2017).
5. Fowkes, F.G.R. et al. Comparison of global estimates of prevalence and risk factors for peripheral artery disease in 2000 and 2010: a systematic review and analysis. *The Lancet* **382**, 1329-1340 (2013).
6. Kullo, I.J. & Rooke, T.W. Peripheral Artery Disease. **374**, 861-871 (2016).
7. Ouriel, K. Peripheral arterial disease. *The Lancet* **358**, 1257-1264 (2001).
8. Graziani, L.J.C.T.O.i.C.M. Comprehensive Approach to Management of Critical Limb Ischemia. **16**, 332 (2014).
9. Marston, W.A. et al. Natural history of limbs with arterial insufficiency and chronic ulceration treated without revascularization. *J. Vasc. Surg.* **44**, 108-114.e101 (2006).
10. Jude, E.B., Eleftheriadou, I. & Tentolouris, N. Peripheral arterial disease in diabetes--a review. *Diabet. Med.* **27**, 4-14 (2010).
11. Thukkani, A.K. & Kinlay, S. Endovascular intervention for peripheral artery disease. *Circ. Res.* **116**, 1599-1613 (2015).
12. Goodney, P.P., Likosky, D.S. & Cronenwett, J.L. Predicting ambulation status one year after lower extremity bypass. *J. Vasc. Surg.* **49**, 1431-1439.e1431 (2009).
13. Grochot-Przeczek, A., Dulak, J. & Jozkowicz, A. Therapeutic angiogenesis for revascularization in peripheral artery disease. *Gene* **525**, 220-228 (2013).
14. Raval, Z. & Losordo, D.W. Cell therapy of peripheral arterial disease: from experimental findings to clinical trials. *Circ. Res.* **112**, 1288-1302 (2013).
15. Medina, R.J. et al. Endothelial Progenitors: A Consensus Statement on Nomenclature. **6**, 1316-1320 (2017).
16. McDonald, A.I. et al. Endothelial Regeneration of Large Vessels Is a Biphasic Process Driven by Local Cells with Distinct Proliferative Capacities. *Cell Stem Cell* **23**, 210-225.e216 (2018).
17. Critser, P.J. & Yoder, M.C. Endothelial colony-forming cell role in neoangiogenesis and tissue repair. *Current opinion in organ transplantation* **15**, 68-72 (2010).
18. Pyšná, A. et al. Endothelial Progenitor Cells Biology in Diabetes Mellitus and Peripheral Arterial Disease and their Therapeutic Potential. (2018).
19. Cai, L. et al. IFATS Collection: Human Adipose Tissue-Derived Stem Cells Induce Angiogenesis and Nerve Sprouting Following Myocardial Infarction, in Conjunction with Potent Preservation of Cardiac Function. **27**, 230-237 (2009).
20. Danoviz, M.E. et al. Rat Adipose Tissue-Derived Stem Cells Transplantation Attenuates Cardiac Dysfunction Post Infarction and Biopolymers Enhance Cell Retention. *PLoS One* **5**, e12077 (2010).
21. Kim, E.-H. & Heo, C.Y. Current applications of adipose-derived stem cells and their future perspectives. *World journal of stem cells* **6**, 65-68 (2014).
22. Weiss, D.J. Stem Cells, Cell Therapies, and Bioengineering in Lung Biology and Diseases. Comprehensive Review of the Recent Literature 2010–2012. **10**, S45-S97 (2013).

23. Magee, Jeffrey A., Piskounova, E. & Morrison, Sean J. Cancer Stem Cells: Impact, Heterogeneity, and Uncertainty. *Cancer Cell* **21**, 283-296 (2012).
24. Inglez, J.C.D. in Vascular Diseases for the Non-Specialist. (eds. T.P. Navarro, A. Dardik, D. Junqueira & L. Cisneros) 233-251 (Springer International Publishing, Cham; 2017).
25. Panyam, J. & Labhasetwar, V. Biodegradable nanoparticles for drug and gene delivery to cells and tissue. *Adv. Drug Del. Rev.* **55**, 329-347 (2003).
26. Rizvi, S.A.A. & Saleh, A.M. Applications of nanoparticle systems in drug delivery technology. *Saudi pharmaceutical journal : SPJ : the official publication of the Saudi Pharmaceutical Society* **26**, 64-70 (2018).
27. Tang, J. et al. Nanomedical Theranostics in Cardiovascular Disease. **5**, 19-25 (2012).
28. Wolfram, J. et al. Safety of Nanoparticles in Medicine. *Curr. Drug Targets* **16**, 1671-1681 (2015).
29. Allen, T.M. & Cullis, P.R. Drug Delivery Systems: Entering the Mainstream. **303**, 1818-1822 (2004).
30. LaVan, D.A., McGuire, T. & Langer, R. Small-scale systems for in vivo drug delivery. *Nat. Biotechnol.* **21**, 1184 (2003).
31. Guo, X. & Szoka, F.C. Chemical Approaches to Triggerable Lipid Vesicles for Drug and Gene Delivery. *Acc. Chem. Res.* **36**, 335-341 (2003).
32. De Jong, W.H. & Borm, P.J.A. Drug delivery and nanoparticles:applications and hazards. *International journal of nanomedicine* **3**, 133-149 (2008).
33. Kuriakose, A.E. et al. in Reference Module in Biomedical Sciences (Elsevier, 2018).
34. Semenza, G.L. Targeting hypoxia-inducible factor 1 to stimulate tissue vascularization. **64**, 361-363 (2016).
35. Stather, P.W. et al. Identification of microRNAs associated with abdominal aortic aneurysms and peripheral arterial disease. **102**, 755-766 (2015).
36. Noukeu, L.C., Wolf, J., Yuan, B., Banerjee, S. & Nguyen, K.T. Nanoparticles for Detection and Treatment of Peripheral Arterial Disease. **14**, 1800644 (2018).
37. De Silva, G.S., Desai, K.A., Semenkovich, C.F., Sanchez, L.A. & Zayed, M.A. Circulating Fatty Acid Synthase Is a Novel Biomarker of Disease Severity in Patients with Peripheral Arterial Disease and Diabetes. *J. Am. Coll. Surg.* **227**, S285-S286 (2018).
38. Höbaus, C. et al. FABP4 and Cardiovascular Events in Peripheral Arterial Disease. **69**, 424-430 (2018).
39. Gao, Y. et al. Controlled nanoparticle release from stable magnetic microbubble oscillations. *Npg Asia Materials* **8**, e260 (2016).
40. Mørch, Ý. et al. Nanoparticle-stabilized microbubbles for multimodal imaging and drug delivery. **10**, 356-366 (2015).
41. Cochran, M.C. et al. Disposition of Ultrasound Sensitive Polymeric Drug Carrier in a Rat Hepatocellular Carcinoma Model. *Acad. Radiol.* **18**, 1341-1348 (2011).
42. Rychak, J.J. & Klibanov, A.L. Nucleic acid delivery with microbubbles and ultrasound. *Adv. Drug Del. Rev.* **72**, 82-93 (2014).
43. Nande, R. et al. Microbubble-assisted p53, RB, and p130 gene transfer in combination with radiation therapy in prostate cancer. *Curr. Gene Ther.* **13**, 163-174 (2013).
44. Boissenot, T., Bordat, A., Fattal, E. & Tsapis, N. Ultrasound-triggered drug delivery for cancer treatment using drug delivery systems: From theoretical considerations to practical applications. *J. Control. Release* **241**, 144-163 (2016).
45. Whitehill, T.A. Role of revascularization in the treatment of claudication. *Vasc. Med.* **2**, 252-256 (1997).
46. Tabibiazar, R. & Rockson, S.G. Angiogenesis and the ischaemic heart. *Eur. Heart J.* **22**, 903-918 (2001).
47. Nessa, A. et al. Angiogenesis-a novel therapeutic approach for ischemic heart disease. *Mymensingh Med. J.* **18**, 264-272 (2009).

48. Collinson, D.J. & Donnelly, R. Therapeutic angiogenesis in peripheral arterial disease: can biotechnology produce an effective collateral circulation? *Eur. J. Vasc. Endovasc. Surg.* **28**, 9-23 (2004).
49. Allen, J.D., Giordano, T. & Kevil, C.G. Nitrite and Nitric Oxide Metabolism in Peripheral Artery Disease. *Nitric Oxide* **26**, 217-222 (2012).
50. Ignarro, L.J., Napoli, C. & Loscalzo, J. Nitric oxide donors and cardiovascular agents modulating the bioactivity of nitric oxide: an overview. *Circ. Res.* **90**, 21-28 (2002).
51. Williams, G. et al. Nitric oxide manipulation: a therapeutic target for peripheral arterial disease? *Cardiol. Res. Pract.* **2012**, 656247 (2012).
52. Forstermann, U. & Sessa, W.C. Nitric oxide synthases: regulation and function. *Eur. Heart J.* **33**, 829-837, 837a-837d (2012).
53. Gkaliagkousi, E. & Ferro, A. Nitric oxide signalling in the regulation of cardiovascular and platelet function. *Front. Biosci. (Landmark Ed.)* **16**, 1873-1897 (2011).
54. Coletta, C. et al. Hydrogen sulfide and nitric oxide are mutually dependent in the regulation of angiogenesis and endothelium-dependent vasorelaxation. *Proc. Natl. Acad. Sci. U. S. A.* **109**, 9161-9166 (2012).
55. Duranski, M.R. et al. Cytoprotective effects of nitrite during in vivo ischemia-reperfusion of the heart and liver. *J. Clin. Invest.* **115**, 1232-1240 (2005).
56. Webb, A. et al. Reduction of nitrite to nitric oxide during ischemia protects against myocardial ischemia-reperfusion damage. *Proc. Natl. Acad. Sci. U. S. A.* **101**, 13683-13688 (2004).
57. Allen, J.D. et al. Plasma nitrite response and arterial reactivity differentiate vascular health and performance. *Nitric Oxide* **20**, 231-237 (2009).
58. Nguyen, M.C. et al. Arginase Inhibition Restores Peroxynitrite-Induced Endothelial Dysfunction via L-Arginine-Dependent Endothelial Nitric Oxide Synthase Phosphorylation. *Yonsei Med. J.* **57**, 1329-1338 (2016).
59. Mayo, J.N. et al. Nitrative stress in cerebral endothelium is mediated by mGluR5 in hyperhomocysteinemia. *J. Cereb. Blood Flow Metab.* **32**, 825-834 (2012).
60. Paik, Y.H. & Brenner, D.A. NADPH oxidase mediated oxidative stress in hepatic fibrogenesis. *Korean J. Hepatol.* **17**, 251-257 (2011).
61. Wang, Y., Chun, O.K. & Song, W.O. Plasma and dietary antioxidant status as cardiovascular disease risk factors: a review of human studies. *Nutrients* **5**, 2969-3004 (2013).
62. Pacurari, M., Kafoury, R., Tchounwou, P.B. & Ndebele, K. The Renin-Angiotensin-aldosterone system in vascular inflammation and remodeling. *Int. J. Inflam.* **2014**, 689360 (2014).
63. Steyers, C.M., 3rd & Miller, F.J., Jr. Endothelial dysfunction in chronic inflammatory diseases. *Int. J. Mol. Sci.* **15**, 11324-11349 (2014).
64. Gori, T. & Parker, J.D. Nitrate-induced toxicity and preconditioning: a rationale for reconsidering the use of these drugs. *J. Am. Coll. Cardiol.* **52**, 251-254 (2008).
65. Liuni, A. et al. Coadministration of atorvastatin prevents nitroglycerin-induced endothelial dysfunction and nitrate tolerance in healthy humans. *J. Am. Coll. Cardiol.* **57**, 93-98 (2011).
66. Feelisch, M., Ostrowski, J. & Noack, E. On the mechanism of NO release from sydnonimines. *J. Cardiovasc. Pharmacol.* **14 Suppl 11**, S13-22 (1989).
67. Acharya, S. et al. Design and synthesis of novel hybrid sydnonimine and prodrug useful for glaucomatous optic neuropathy. *Bioorg. Med. Chem. Lett.* **26**, 1490-1494 (2016).
68. Le, D.Q., Kuriakose, A.E., Nguyen, D.X., Nguyen, K.T. & Acharya, S. Hybrid Nitric Oxide Donor and its Carrier for the Treatment of Peripheral Arterial Diseases. *Sci. Rep.* **7**, 8692 (2017).
69. Chen, Z., Zhang, J. & Stamler, J.S. Identification of the enzymatic mechanism of nitroglycerin bioactivation. *Proc. Natl. Acad. Sci. U. S. A.* **99**, 8306-8311 (2002).
70. Masuda, K., Imashiro, Y. and Kaneko, T. Mesoionic compounds. I. Synthesis of 3-dialkylaminosydnonimines. *Chem. Pharm. Bull.* **18**, 128-132 (1970).

71. Haj-Yehia, A. et al. Development of 3-nitratomethyl-PROXYL (NMP): A novel, bifunctional superoxide dismutase-mimic-nitric oxide-donor. *Drug Dev. Res.* **50**, 528-536 (2000).
72. Koppolu, B., Rahimi, M., Nattama, S., Wadajkar, A. & Nguyen, K.T. Development of multiple-layer polymeric particles for targeted and controlled drug delivery. *Nanomedicine* **6**, 355-361 (2010).
73. Shah, B., Kona, S., Gilbertson, T.A. & Nguyen, K.T. Effects of poly-(lactide-co-glycolide) nanoparticles on electrophysiological properties of enteroendocrine cells. *J Nanosci Nanotechnol* **11**, 3533-3542 (2011).
74. Menon, J.U. et al. Effects of surfactants on the properties of PLGA nanoparticles. *J. Biomed. Mater. Res. A* **100**, 1998-2005 (2012).
75. Wadajkar, A.S. et al. Multifunctional particles for melanoma-targeted drug delivery. *Acta Biomater.* **8**, 2996-3004 (2012).
76. Patel, R.H. et al. Multifunctionality of indocyanine green-loaded biodegradable nanoparticles for enhanced optical imaging and hyperthermia intervention of cancer. *J. Biomed. Opt.* **17**, 046003 (2012).
77. Menon, J.U. et al. Polymeric nanoparticles for pulmonary protein and DNA delivery. *Acta Biomater.* **10**, 2643-2652 (2014).
78. Menon, J.U., Tumati, V., Hsieh, J.T., Nguyen, K.T. & Saha, D. Polymeric nanoparticles for targeted radiosensitization of prostate cancer cells. *J. Biomed. Mater. Res. A* **103**, 1632-1639 (2015).
79. Kona, S. et al. Targeted biodegradable nanoparticles for drug delivery to smooth muscle cells. *J Nanosci Nanotechnol* **12**, 236-244 (2012).
80. Goodfriend, A.C. et al. Thermally processed polymeric microparticles for year-long delivery of dexamethasone. *Mater. Sci. Eng. C Mater. Biol. Appl.* **58**, 595-600 (2016).
81. Ostergaard, L. et al. Diminished NO release in chronic hypoxic human endothelial cells. *American journal of physiology. Heart and circulatory physiology* **293**, H2894-2903 (2007).
82. Cianfarani, F. et al. Diabetes impairs adipose tissue-derived stem cell function and efficiency in promoting wound healing. *Wound Repair Regen.* **21**, 545-553 (2013).
83. Lau, K.M. et al. Synergistic interaction between Astragali Radix and Rehmanniae Radix in a Chinese herbal formula to promote diabetic wound healing. *J. Ethnopharmacol.* **141**, 250-256 (2012).
84. Khazaei, M., Salehi, E., Rashidi, B., Javanmard, S.H. & Fallahzadeh, A.R. Role of peroxisome proliferator-activated receptor beta agonist on angiogenesis in hindlimb ischemic diabetic rats. *J. Diabetes Complications* **26**, 137-140 (2012).
85. Johnson, D. Endothelial damage due to ischemia and reperfusion is prevented with SIN-1. *Cardiovasc. Surg.* **6**, 367-372 (1998).
86. Shin, W.S. et al. Nitric oxide attenuates vascular smooth muscle cell activation by interferon-gamma. The role of constitutive NF-kappa B activity. *J. Biol. Chem.* **271**, 11317-11324 (1996).
87. Lei, J., Vodovotz, Y., Tzeng, E. & Billiar, T.R. Nitric oxide, a protective molecule in the cardiovascular system. *Nitric Oxide* **35**, 175-185 (2013).
88. Maruhashi, T. et al. Critical role of exogenous nitric oxide in ROCK activity in vascular smooth muscle cells. *PLoS One* **9**, e109017 (2014).
89. Fiuza, B. et al. Impact of SIN-1-derived peroxynitrite flux on endothelial cell redox homeostasis and bioenergetics: protective role of diphenyl diselenide via induction of peroxiredoxins. *Free Radic. Res.* **49**, 122-132 (2015).
90. Oishi, J.C. et al. In vitro Treatment with cis-[Ru(H-dcbpy-)2(Cl)(NO)] Improves the Endothelial Function in Aortic Rings with Endothelial Dysfunction. *J. Pharm. Pharm. Sci.* **18**, 696-704 (2015).
91. Sadowska-Bartosz, I., Gajewska, A., Skolimowski, J., Szewczyk, R. & Bartosz, G. Nitroxides protect against peroxynitrite-induced nitration and oxidation. *Free Radic. Biol. Med.* **89**, 1165-1175 (2015).

92. Park, H.S. et al. Beneficial effect of a nitric oxide donor in an ex vivo model of pig-to-human pulmonary xenotransplantation. *Xenotransplantation* **22**, 391-398 (2015).
93. Das, A. et al. Reversal of SIN-1-induced eNOS dysfunction by the spin trap, DMPO, in bovine aortic endothelial cells via eNOS phosphorylation. *Br. J. Pharmacol.* **171**, 2321-2334 (2014).
94. Dong, Y. et al. Nitrative Stress Participates in Endothelial Progenitor Cell Injury in Hyperhomocysteinemia. *PLoS One* **11**, e0158672 (2016).
95. Kwon, B. et al. H2O2-responsive antioxidant polymeric nanoparticles as therapeutic agents for peripheral arterial disease. *Int. J. Pharm.* **511**, 1022-1032 (2016).
96. FOTIS, L. et al. Intercellular Adhesion Molecule (ICAM)-1 and Vascular Cell Adhesion Molecule (VCAM)-1 at the Early Stages of Atherosclerosis in a Rat Model. **26**, 243-250 (2012).
97. Adams, William J. et al. Functional Vascular Endothelium Derived from Human Induced Pluripotent Stem Cells. *Stem Cell Reports* **1**, 105-113 (2013).
98. Kochi, T. et al. Characterization of the Arterial Anatomy of the Murine Hindlimb: Functional Role in the Design and Understanding of Ischemia Models. *PLoS One* **8**, e84047 (2014).
99. Pellegrin, M. et al. Experimental peripheral arterial disease: new insights into muscle glucose uptake, macrophage, and T-cell polarization during early and late stages. *Physiological Reports* **2**, e00234 (2014).
100. Tebebi, P.A. et al. Improving the therapeutic efficacy of mesenchymal stromal cells to restore perfusion in critical limb ischemia through pulsed focused ultrasound. *Sci. Rep.* **7**, 41550-41550 (2017).
101. Ma, X.-T. et al. Effect of Content of Sulfate Groups in Seaweed Polysaccharides on Antioxidant Activity and Repair Effect of Subcellular Organelles in Injured HK-2 Cells %J Oxidative Medicine and Cellular Longevity. **2017**, 13 (2017).
102. Seedevi, P., Moovendhan, M., Vairamani, S. & Shanmugam, A. Evaluation of antioxidant activities and chemical analysis of sulfated chitosan from Sepia prashadi. *Int. J. Biol. Macromol.* **99**, 519-529 (2017).
103. Xing, R. et al. Antioxidant activity of differently regioselective chitosan sulfates in vitro. *Bioorg. Med. Chem.* **13**, 1387-1392 (2005).

BIOGRAPHY

Duong Le started his enthusiasm for STEM early in the secondary school, particularly in mathematics and chemistry. This led him to joined the gifted program in Chemistry and Chemical Engineering in High school and College, respectively, in Vietnam. Since then, it has shaped his desire for an academic career in the future, where he wished to be a successful professor in field. Motivated by his father's death of cardiovascular disease during his college, he joined Biomedical and Nanomaterials Laboratory of the national key laboratories at Vietnam Academy for Science and Technology in 2010. Under supervision or top leading professors, XuanPhuc (Benedict) Nguyen, Lam Tran and Thu Ha, he investigated comprehensively targeting drug delivery systems to treat lung cancers, the one that took away his uncle's life. At the same time, he completed his Master of Science in Biotechnology-Pharmacology in 2012 in preparation for his long-term career. Next, he joined the Department of Bioengineering at the University of Texas at Arlington in the Fall of 2014 and found a great match in Laboratory for Nanomedicine and Drug Delivery, led by professor Kytai Truong Nguyen. Here he has not only been sharpened his critical thinking but also expanded his mind to pursue many cutting-edge researches. He has investigated the development of drug delivery systems for breast cancer, diabetic wound healing, and especially peripheral arterial diseases. His research was again fueled with the initial motivation. Additionally, he was enriched his academic experiences through network collaboration, mentorship and lecturing.

Upon completing Doctor of Philosophy degree in Biomedical Engineering from University of Texas at Arlington, Mr. Le is going further toward the development of alternative treatments for cardiovascular diseases. It has always been his dream to be a successful professor in this field.